

Pseudo-Goldstone modes and dynamical gap generation from order-by-thermal-disorder

Subhankar Khatua,^{1,2} Michel J. P. Gingras,² and Jeffrey G. Rau¹

¹*Department of Physics, University of Windsor, 401 Sunset Avenue, Windsor, Ontario, N9B 3P4, Canada*

²*Department of Physics and Astronomy, University of Waterloo, Waterloo, Ontario, N2L 3G1, Canada*

(Dated: January 31, 2023)

Accidental ground state degeneracies – those not a consequence of global symmetries of the Hamiltonian – are inevitably lifted by fluctuations, often leading to long-range order, a phenomenon known as “order-by-disorder” (ObD). The detection and characterization of ObD in real materials currently lacks clear, qualitative signatures that distinguish ObD from conventional energetic selection. We show that for order-by-*thermal*-disorder (ObTD) such a signature exists: a characteristic temperature dependence of the fluctuation-induced pseudo-Goldstone gap. We demonstrate this in a minimal two-dimensional model that exhibits ObTD, the ferromagnetic Heisenberg-compass model on a square lattice. Using spin-dynamics simulations and self-consistent mean-field calculations, we determine the pseudo-Goldstone gap, Δ , and show that at low temperatures it scales as the square root of temperature, \sqrt{T} . We establish that a power-law temperature dependence of the gap is a general consequence of ObTD, showing that all key features of this physics can be captured in a simple model of a particle moving in an effective potential generated by the fluctuation-induced free energy.

Strongly competing interactions, or frustration, enhance quantum and thermal fluctuations, and undermine the development of conventional magnetic order. The latter can even be prevented entirely down to zero temperature, leading to classical [1–3] or quantum spin liquids [4–10]. However, additional perturbative interactions can relieve the frustration and favor the development of long-range order (LRO). Accordingly, the majority of spin liquid candidates ultimately evade fate as a spin liquid [8, 11]. The ability of these interactions, inconsequential without frustration, to dictate the ground state and low-temperature properties of a system is at the root of the plethora of exotic phenomena displayed by highly-frustrated magnetic materials [10, 12–18].

This relief of frustration is not always complete. Instead of an extensively degenerate manifold, a system can possess a sub-extensive *accidental* ground state degeneracy, unprotected by symmetry. Classically, this degeneracy can be robust to a range of realistic interactions including symmetry-allowed two-spin exchange [19]. Here, the role of fluctuations is dramatically changed: instead of being detrimental, they can lift the classical degeneracy and stabilize order – this is the celebrated phenomenon of *order-by-disorder* (ObD) [20–22]. While numerous theoretical models have been proposed [20–33], there is a paucity of real materials that unambiguously harbor ObD [19, 34–37]. The standard strategy for experimental confirmation is indirect, relying on parametrizing a theoretical model of the material, establishing ObD within that model, and then validating its predictions for the ordered state experimentally.

While this program has been applied somewhat successfully to a handful of materials [19, 34–37], the inability to evince ObD directly, without relying on detailed modelling, highlights something lacking in our understanding of ObD. Clear *qualitative*, model-independent signatures are needed; for example, experimental observation of characteristic power-laws in heat capacity or transport can diagnose the character of low-energy excitations, such as exchange statistics, dimensionality or their dispersion relations [9, 11, 38, 39]. Does the presence of ObD exhibit a “smoking-gun” experimental signature? This can be difficult or subtle to discern.

For ObD from quantum fluctuations [21], the formation of an ObD spin-wave gap is generally not distinguishable from one induced energetically by multi-spin interactions [40–42].

In this Letter, we identify a clear signature of order-by-*thermal*-disorder (ObTD): a dynamically generated gap growing as the square root of temperature. We investigate this gapped “pseudo-Goldstone” (PG) mode [44–46] in a minimal 2D classical spin model exhibiting ObTD, the ferromagnetic Heisenberg-compass model on a square lattice, belonging to a class of models relevant to Mott insulators with strong spin-orbit coupling [47–55]. Through spin-dynamics simulations, we determine the PG gap, Δ , and show it varies with temperature as $\Delta \propto \sqrt{T}$, in quantitative agreement with self-consistent mean-field theory (SCMFT). This mode is well-defined, with the linewidth, Γ , due to thermal broadening, $\Gamma \propto T^2 \ll \Delta$. We further demonstrate that our key results can be captured by an effective description of a particle moving in a potential generated by the fluctuation-induced free energy. Using this picture, we argue that the temperature dependence of the PG gap, \sqrt{T} (T) for type-I (II) PG modes [56], is *universal*, applicable to *any* system exhibiting ObTD. Finally, due to the low dimensionality [57], ObTD faces a subtle competition against potentially infrared-divergent fluctuations [58, 59]. While ObTD ultimately prevails, and true LRO develops, the magnetization displays logarithmic corrections at low temperature, a remnant of the diverging infrared fluctuations.

Model.— We consider the *classical* ferromagnetic Heisenberg-compass model on a square lattice

$$\mathcal{H} = \sum_{\mathbf{r}} \left[-J \sum_{\delta=\hat{x},\hat{y}} \mathbf{S}_{\mathbf{r}} \cdot \mathbf{S}_{\mathbf{r}+\delta} - K \left(S_{\mathbf{r}}^x S_{\mathbf{r}+\hat{x}}^x + S_{\mathbf{r}}^y S_{\mathbf{r}+\hat{y}}^y \right) \right], \quad (1)$$

where $\mathbf{S}_{\mathbf{r}} \equiv (S_{\mathbf{r}}^x, S_{\mathbf{r}}^y, S_{\mathbf{r}}^z)$ is a unit vector at site \mathbf{r} , and $\delta = \hat{x}, \hat{y}$ denote the nearest-neighbor bond directions. We consider ferromagnetic Heisenberg and compass interactions with $J > 0$, $K > 0$ (see SM [60] for a discussion of other signs) and with J the unit of energy, setting $J \equiv \hbar \equiv k_B \equiv 1$ throughout.

For $K = 0$, the model [Eq.(1)] is the well-known Heisenberg ferromagnet with uniform ferromagnetic ground states of arbitrary direction, $\mathbf{S}_{\mathbf{r}} = \hat{\mathbf{n}}$, related by global spin-rotation

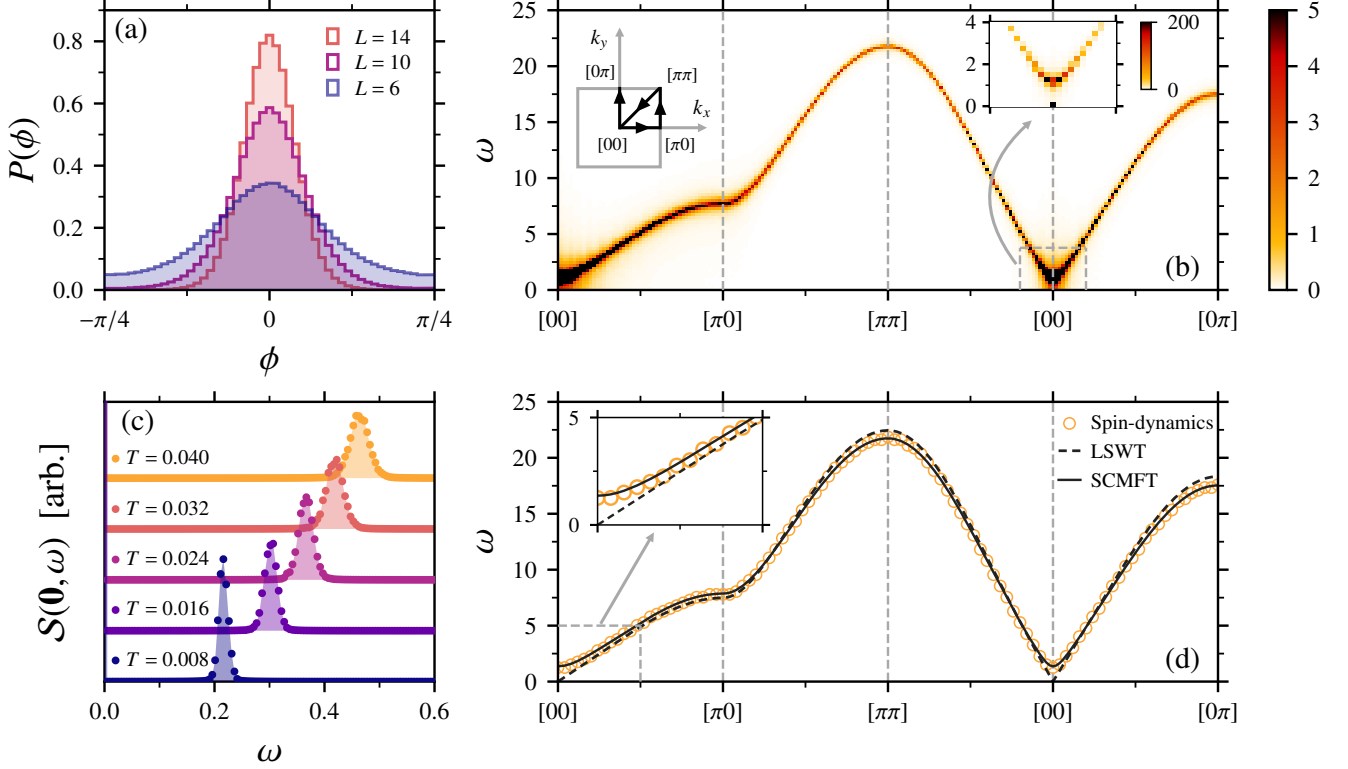


FIG. 1. (a) Probability distribution, $P(\phi)$, of the angle, ϕ , characterizing the direction of the net magnetization obtained using MC simulations with $K = 5$ at $T = 0.4$ for several system sizes, L . Due to C_4 symmetry, $P(\phi)$ is shown for $\phi \in [-\pi/4, \pi/4]$. (b) Dynamical structure factor, $S(\mathbf{k}, \omega)$ obtained from spin-dynamics simulations for $L = 100$ with $K = 5$ at $T = 0.4$ along a path through the Brillouin zone (see left inset). Overall intensity is arbitrary. (Right inset) Spectrum near $[00]$ showing the PG gap [43]. (c) Dynamical structure factor at $\mathbf{k} = \mathbf{0}$, $S(\mathbf{0}, \omega)$, obtained from spin-dynamics simulations for $L = 40$ at various temperatures with $K = 5$. Overall intensity is arbitrary. (d) Excitation spectrum along the same path as in panel-(b) from the LSWT, SCMFT, and spin-dynamics simulations with $K = 5$ for $L = 100$ at $T = 0.4$. The spin-dynamics spectrum tracks the frequencies of maximum of $S(\mathbf{k}, \omega)$. The inset highlights a small region near $[00]$, showing the PG mode.

symmetry. For $K > 0$, this symmetry is absent and \mathcal{H} in Eq. (1) is minimized by any uniform magnetization in the $\hat{\mathbf{x}} - \hat{\mathbf{y}}$ plane. These ground states are characterized by an angle $\phi \in [0, 2\pi)$ with $\mathbf{S}_r = \cos \phi \hat{\mathbf{x}} + \sin \phi \hat{\mathbf{y}}$. Unlike the pure Heisenberg ferromagnet, these are only *accidentally* degenerate, as the continuous in-plane spin rotations connecting them do not preserve the anisotropic compass term. However, a discrete C_4 symmetry about the $\hat{\mathbf{z}}$ axis and C_2 symmetries about the $\hat{\mathbf{x}}$ and $\hat{\mathbf{y}}$ axes still remain.

Simulations.— We first show that this model exhibits ObTD via Monte Carlo (MC) simulations on a lattice with $N = L^2$ sites. To expose the state selection, we construct a probability distribution for magnetization direction, encoded in ϕ , $P(\phi)$, using a sample of thermalized states (see SM [60]). As shown in Fig. 1(a), $P(\phi)$ exhibits maxima at $\phi = 0, \pi/2, \pi, 3\pi/2$, corresponding to ferromagnetic ground states with $\hat{\mathbf{n}}$ along the $\pm\hat{\mathbf{x}}, \pm\hat{\mathbf{y}}$ directions. At low temperatures, fluctuations thus select four discrete ground states via ObTD from a one-parameter manifold of states.

We now consider the classical dynamics to examine the associated PG mode. The equation of motion for the classical spins is the Landau-Lifshitz equation [61], $d\mathbf{S}_i/dt = \mathbf{B}_r \times \mathbf{S}_r$,

describing precession about the exchange field, \mathbf{B}_r , produced by neighboring spins

$$\mathbf{B}_r \equiv - \sum_{\delta=\pm\hat{\mathbf{x}}, \pm\hat{\mathbf{y}}} [J\mathbf{S}_{r+\delta} + K\mathbf{S}_{r+\delta}^\delta]. \quad (2)$$

Starting with states drawn via MC sampling at temperature T , we numerically integrate the Landau-Lifshitz equations, and compute the dynamical structure factor, $S(\mathbf{k}, \omega) = \langle |\mathbf{S}_k(\omega)|^2 \rangle$, where $\mathbf{S}_k(\omega)$ is the Fourier transform of spins, and $\langle \dots \rangle$ denotes averaging over the initial states [60]. Results for $S(\mathbf{k}, \omega)$ at a representative T and K [60] are shown in Fig. 1(b), exhibiting sharp spin-waves with a *nearly* gapless mode at $\mathbf{k} = \mathbf{0}$. Closer examination reveals a well-defined gap, as highlighted in the top right inset of Fig. 1(b) – this is the PG gap.

To determine the PG gap *quantitatively*, we consider a cut of the structure factor at $\mathbf{k} = \mathbf{0}$, i.e., $S(\mathbf{0}, \omega)$. As the PG gap is much smaller than the bandwidth of the spectrum [see Fig. 1(b)], a significantly higher frequency resolution is required to accurately compute the gap [60], so a much longer integration time window is necessary. Cuts, $S(\mathbf{0}, \omega)$, for several temperatures are presented in Fig. 1(c), with the peak lo-

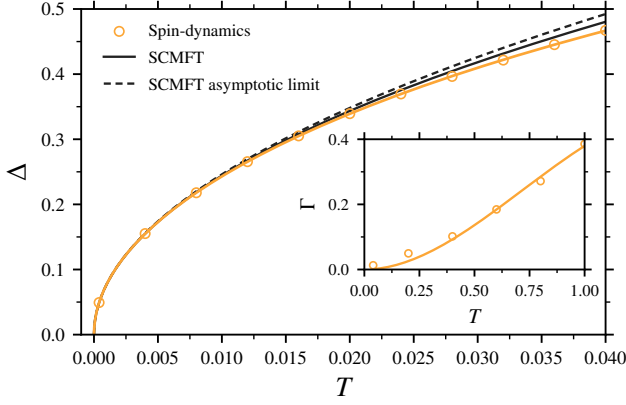


FIG. 2. Pseudo-Goldstone gap, Δ , as a function of temperature from spin-dynamics simulations with $K = 5$. The data is well-described by the fit $\Delta = 2.46242 \sqrt{T} - 3.21907 T^{3/2}$. The SCMFT gap agrees with it quantitatively and provides the asymptotic $T \rightarrow 0$ scaling, $2.46147 \sqrt{T}$. (Inset) Linewidth of the PG mode, Γ , as a function of temperature from spin-dynamics simulations. It is well described by the fit, $\Gamma = 0.709286 T^2 - 0.329751 T^3$. All data have been extrapolated in the system size to the thermodynamic limit [60].

cation indicating the PG gap (see SM [60]). The temperature dependence of Δ is shown in Fig. 2. The leading contribution to the PG gap scales as the *square root* of temperature, vanishing as $T \rightarrow 0$, and is well-described by the fit $\Delta \sim 2.46 \sqrt{T}$.

The thermal broadening of the spectrum induces a finite width to all excitations, including the PG mode. The PG mode linewidth, Γ , can be obtained from the full-width at half maximum of $S(\mathbf{0}, \omega)$ [see Fig. 1(c)] as a function of temperature. The inset in Fig. 2 shows that $\Gamma \propto T^2$ at low temperatures (see SM [60]). Since $\Gamma \ll \Delta$ as $T \rightarrow 0$, this PG mode is well-defined.

Spin-wave analysis.— The simulations have revealed that the system has LRO and hosts a PG excitation, where the PG gap and linewidth scale with temperature as \sqrt{T} and T^2 , respectively. To understand how these scaling laws arise, we consider a spin-wave analysis about the ordered state [62]. Since tackling spin-wave interactions is difficult within a purely classical approach [63–65], we follow the more widely used and computationally convenient quantum spin-wave analysis [66–68], taking the classical limit only at the end.

We first discuss the spectrum and state selection due to ObTD in linear spin-wave theory (LSWT). Expanding about a classical ground state (parametrized by ϕ) using the Holstein-Primakoff (HP) transformation [62], we obtain to $O(S)$

$$\mathcal{H}_2 = \sum_{\mathbf{k}} \left[A_{\mathbf{k}} a_{\mathbf{k}}^\dagger a_{\mathbf{k}} + \frac{1}{2!} (B_{\mathbf{k}} a_{\mathbf{k}}^\dagger a_{-\mathbf{k}}^\dagger + \text{H.c.}) \right], \quad (3)$$

where $a_{\mathbf{k}}$ denotes the bosonic annihilation operator at wave vector \mathbf{k} , and $A_{\mathbf{k}}$ and $B_{\mathbf{k}}$ depend on ϕ , J , and K (see SM [60]). \mathcal{H}_2 in Eq. (3) can be diagonalized by a Bogoliubov transformation [62], giving spin-wave energies $\omega_{\mathbf{k}} = \sqrt{A_{\mathbf{k}}^2 - B_{\mathbf{k}}^2}$. As

the spectrum depends on the ground state angle ϕ , fluctuations can lift the accidental classical degeneracy. To examine state selection due to ObTD, we search for the ground states where the free energy is minimal. Starting with the quantum free energy $F_{\text{qu}} = \frac{1}{2} \sum_{\mathbf{k}} \omega_{\mathbf{k}} + T \sum_{\mathbf{k}} \ln(1 - e^{-\omega_{\mathbf{k}}/T})$, the classical limit $T \gg \omega_{\mathbf{k}}$ yields $F = T \sum_{\mathbf{k}} \ln \omega_{\mathbf{k}}$ [69]. This classical free energy has four minima at $\phi = 0, \pi/2, \pi, 3\pi/2$ – establishing selection by ObTD, in agreement with the MC results.

Within LSWT, quantum and classical calculations give the same spectrum, $\omega_{\mathbf{k}}$ [22]. This spectrum, calculated about $\phi = 0$, exhibits a gapless mode at $\mathbf{k} = \mathbf{0}$ as shown in Fig. 1(d). To obtain a PG gap, spin-wave interactions must be included, as we next discuss.

Interacting spin waves.— Performing the HP expansion to next order in $1/S$, the LSWT Hamiltonian [Eq. (3)] is augmented by interaction terms. Three-boson interactions are absent due to a C_2 symmetry about the ordering direction, leaving only terms quartic in the bosons at $O(S^0)$ (see SM [60]). To treat this interacting problem, we adopt a mean-field approach [66, 67], decoupling the quartic terms into products of quadratic terms and thermal averages of two-boson operators. Following this procedure, the new effective quadratic Hamiltonian mirrors Eq. (3), but with $A_{\mathbf{k}}$ and $B_{\mathbf{k}}$ replaced with $(A_{\mathbf{k}} + \delta A_{\mathbf{k}})$ and $(B_{\mathbf{k}} + \delta B_{\mathbf{k}})$. These corrections are

$$\begin{aligned} \delta A_{\mathbf{k}} &= \frac{1}{N} \sum_{\mathbf{q}} \left[V_{\mathbf{k}, \mathbf{q}, \mathbf{0}} \langle a_{\mathbf{q}}^\dagger a_{\mathbf{q}} \rangle + \frac{1}{2} (D_{\mathbf{q}, -\mathbf{q}, \mathbf{k}} \langle a_{\mathbf{q}}^\dagger a_{-\mathbf{q}}^\dagger \rangle + \text{c.c.}) \right], \\ \delta B_{\mathbf{k}} &= \frac{1}{N} \sum_{\mathbf{q}} \left[D_{\mathbf{k}, -\mathbf{k}, \mathbf{q}} \langle a_{\mathbf{q}}^\dagger a_{\mathbf{q}} \rangle + \frac{1}{2} V_{\mathbf{q}, -\mathbf{q}, \mathbf{k}-\mathbf{q}} \langle a_{\mathbf{q}} a_{-\mathbf{q}} \rangle \right], \end{aligned} \quad (4)$$

where $V_{\mathbf{k}_1, \mathbf{k}_2, \mathbf{k}_3}$ and $D_{\mathbf{k}_1, \mathbf{k}_2, \mathbf{k}_3}$ are the coefficients for the 2-2 and 3-1 magnon scattering terms at $O(S^0)$ [60], and $\langle \dots \rangle$ is a thermal average. When these averages are computed using LSWT [Eq. (3)], the corrections [Eq. (4)] reproduce leading order perturbation theory [70, 71]. However, because of the gapless mode, these individual $\delta A_{\mathbf{k}}$ and $\delta B_{\mathbf{k}}$ diverge in the classical limit and perturbation theory breaks down [60].

To resolve these divergences, we perform the averages in Eq. (4) using SCMFT, obtaining a renormalized spectrum, $\Omega_{\mathbf{k}}$ (see SM [60]). Explicitly, $\langle a_{\mathbf{q}}^\dagger a_{\mathbf{q}} \rangle$ and $\langle a_{\mathbf{q}}^\dagger a_{-\mathbf{q}}^\dagger \rangle$ are, classically, computed self-consistently (until convergence) using Eq. (4) and

$$\langle a_{\mathbf{k}}^\dagger a_{\mathbf{k}} \rangle = \frac{T(A_{\mathbf{k}} + \delta A_{\mathbf{k}})}{\Omega_{\mathbf{k}}^2}, \quad \langle a_{\mathbf{k}} a_{-\mathbf{k}} \rangle = -\frac{T(B_{\mathbf{k}} + \delta B_{\mathbf{k}})}{\Omega_{\mathbf{k}}^2}, \quad (5)$$

where $\Omega_{\mathbf{k}} = \sqrt{(A_{\mathbf{k}} + \delta A_{\mathbf{k}})^2 - (B_{\mathbf{k}} + \delta B_{\mathbf{k}})^2}$ and $\langle a_{\mathbf{k}} a_{-\mathbf{k}} \rangle = \langle a_{\mathbf{k}}^\dagger a_{-\mathbf{k}}^\dagger \rangle$.

The SCMFT spectrum $\Omega_{\mathbf{k}}$, plotted in Fig. 1(d), exhibits a clear gap at $\mathbf{k} = \mathbf{0}$. The PG mode, gapless in LSWT, has now become gapped due to magnon-magnon interactions. Excellent agreement between the spectra from SCMFT and spin-dynamics simulations is observed across the full Brillouin zone [see Fig. 1(d)]. The temperature dependences of Δ from the two approaches in Fig. 2 agree quantitatively, with identical \sqrt{T} scaling as $T \rightarrow 0$. This is a key result of this work, establishing a clear spectral *signature* of ObTD.

While the SCMFT is successful in describing the excitation energies, it does not address thermal broadening, since δA_k and δB_k are real, giving an infinite magnon lifetime. To obtain a finite linewidth, perturbation theory must be carried out to higher order. We expect that $\delta A_0 \equiv \delta A_{k=0}$ and $\delta B_0 \equiv \delta B_{k=0}$, interpreted as contributions to the magnon self-energy [60], can be expanded in T as $\delta A_0 = a_1 T + a_2 T^2 + \dots$ and $\delta B_0 = b_1 T + b_2 T^2 + \dots$. Since $|A_0| = |B_0|$, reflecting the gapless LSWT spectrum, and a_1, b_1 [the $O(T)$ corrections in Eq. (4)] are real; any imaginary part, and thus finite lifetime, must arise from a_2 or b_2 . Expanding $\Omega_0 \equiv \Omega_{k=0}$ in T yields $\text{Im} \Omega_0 \approx (\text{Im} a_2) T^2 + \dots$ (see SM [60]). The real part, $\text{Re} \Omega_0$, maintains its leading \sqrt{T} dependence (providing the PG gap) while $\text{Im} \Omega_0$, giving the linewidth, has a leading T^2 dependence, consistent with the simulation results (see inset of Fig. 2).

Effective description.— We now present an effective description capturing the key aspects of the PG mode in a significantly simpler language and with broader applicability, adapting an approach formulated for order-by-quantum-disorder (ObQD) [72]. We consider small uniform deviations from a classical ground state (say $\phi = 0$) with $S_r \approx (\sqrt{1 - \phi^2 - \theta^2}, \phi, \theta)$, accurate to quadratic order in ϕ and θ , where ϕ is the soft mode and θ its conjugate momentum. For small ϕ and θ , $\phi \approx \frac{1}{N} \sum_r S_r^y$ and $\theta \approx \frac{1}{N} \sum_r S_r^z$, with Poisson bracket $\{\phi, \theta\} = 1/N$. For this configuration, we define an effective free energy $F_{\text{eff}}(\theta, \phi) = E_{\text{cl}}(\theta) - TS(\phi)$, where $E_{\text{cl}}(\theta)$ is the classical cost of nonzero θ and $S(\phi) = -\sum_k \ln \omega_k(\phi)$ is the entropy. For small θ and ϕ , F_{eff} can be expanded as $F_{\text{eff}} \approx \frac{1}{2} N (C_\theta \theta^2 + C_\phi \phi^2)$, where $C_\theta = (\partial^2 F_{\text{eff}} / \partial \theta^2) / N = 2K$ and $C_\phi = (\partial^2 F_{\text{eff}} / \partial \phi^2) / N$. Taking F_{eff} as an effective Hamiltonian, the equations of motion [73] for θ and ϕ are

$$\frac{\partial \phi}{\partial t} = +\frac{1}{N} \frac{\partial F_{\text{eff}}}{\partial \theta} = +C_\theta \theta, \quad \frac{\partial \theta}{\partial t} = -\frac{1}{N} \frac{\partial F_{\text{eff}}}{\partial \phi} = -C_\phi \phi, \quad (6)$$

describing a harmonic oscillator. We identify the PG gap as its frequency, $\Delta = \sqrt{C_\theta C_\phi}$. Remarkably, the \sqrt{T} dependence of the PG gap is recovered, since C_ϕ is $O(T)$ and C_θ is $O(1)$. The curvature C_ϕ can be calculated within LSWT, yielding a frequency $2.46147 \sqrt{T}$ for $K = 5$ – exactly the PG gap found in SCMFT as $T \rightarrow 0$ and in agreement with the spin-dynamics simulations (see Fig. 2).

While formulated for the Heisenberg-compass model, this line of argument can be deployed to obtain the PG gap for *any* spin model exhibiting ObTD. A proof of this statement, following the strategy of Ref. [72], will be reported elsewhere [74]. For type-I PG modes ($\omega \propto |k|$, as in the Heisenberg-compass model) $\Delta \propto \sqrt{T}$, while for type-II modes ($\omega \propto |k|^2$), both C_θ, C_ϕ are $O(T)$ and thus $\Delta \propto T$.

Consequences of MWH divergence.— The ability to obtain the PG gap from LSWT presents a puzzle: the perturbative corrections δA_0 and δB_0 diverge logarithmically with system size [57], just as in the MWH theorem [58, 59]. How then do the curvatures of F_{eff} avoid these singularities and give the correct scaling? An analysis of the infrared divergences [60] shows that while δA_0 and δB_0 are singular, $\delta A_0 + \delta B_0$, which determines the leading contribution to the PG gap, is *finite*,

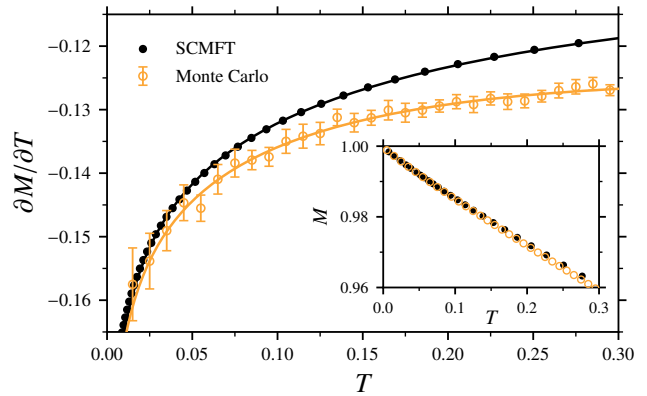


FIG. 3. Derivative of magnetization with respect to temperature, $\partial M / \partial T$, as a function of temperature for $L = 60$, $K = 5$ using MC simulation and SCMFT. MC data is well-described by a fit motivated by SCMFT [60], $-0.09815 - 0.03563T + 0.01485 \ln T$. A similar fit to SCMFT data yields $-0.09631 - 0.01494T + 0.01491 \ln T$. The inset shows M as a function of temperature for the same parameters. MC error bars on M are smaller than the symbol size.

and reproduces the result from Eq. (6). However, divergences in higher order terms do not cancel, and must be cured self-consistently [60].

While these divergences are mostly benign for the PG gap, they appear more dramatically in other quantities, like the magnetization, $M = 1 - \frac{1}{N} \sum_k \langle a_k^\dagger a_k \rangle$. Here, the thermal population, $\langle a_k^\dagger a_k \rangle$ diverges in LSWT, rendering SCMFT necessary to obtain meaningful results. In SCMFT, the PG gap provides an infrared cutoff $\ell \sim 1/\Delta \propto 1/\sqrt{T}$, giving a logarithmic contribution to M scaling as $\propto T \ln T$ as $T \rightarrow 0$ [60]. The presence of this term can be diagnosed from $\partial M / \partial T$, which exhibits a logarithmic singularity as $T \rightarrow 0$ for both the MC simulations and SCMFT (see Fig. 3).

Outlook.— Our analysis of the PG gap will provide a deeper understanding of real materials exhibiting ObD. The existence of PG modes has been used to diagnose ObD, for example in the compounds $\text{Fe}_2\text{Ca}_3(\text{GeO}_4)_3$ [34], $\text{Sr}_2\text{Cu}_3\text{O}_4\text{Cl}_2$ [35] and $\text{Er}_2\text{Ti}_2\text{O}_7$ [36, 41, 75]. In such materials, the ObQD gap likely dominates the ObTD-induced gap discussed in this work. However, in systems where the effect of ObQD is weak or the degrees of freedom are sufficiently classical, ObTD can resurface as the leading selection effect. For example, our results may shed light on the rapidly growing family of two-dimensional van der Waals (vdW) ferromagnets [76–78] where the ObQD gap is expected to be small and thus the gap induced by thermal fluctuations may be more significant. Additionally, while reaching the classical thermal regime is challenging in magnetic materials (due to small spin length S), it may be more accessible in other platforms such as those involving lattice vibrations [79, 80], dipole-coupled nanoconfined molecular rotors [81–84] or artificial mesoscale magnetic crystals [85–88]. Whether ObTD can be realized in such topological systems, and how to detect the temperature dependent PG gap, are open questions; our approach provides a theoret-

ical framework and guidance for future experimental studies in this promising area of research.

ACKNOWLEDGMENTS

We thank Itamar Aharony, Kristian Tyn Kai Chung, Alex Hickey, Daniel Lozano-Gómez, and Darren Pereira for useful discussions. We acknowledge the use of computational resources provided by Digital Research Alliance of Canada. This research was funded by the NSERC of Canada (MJPG, JGR) and the Canada Research Chair Program (MJPG, Tier I).

-
- [1] P. W. Anderson, “Ordering and antiferromagnetism in ferrites,” *Phys. Rev.* **102**, 1008–1013 (1956).
- [2] Jacques Villain, “Insulating spin glasses,” *Zeitschrift für Physik B Condensed Matter* **33**, 31–42 (1979).
- [3] R. Moessner and J. T. Chalker, “Low-temperature properties of classical geometrically frustrated antiferromagnets,” *Phys. Rev. B* **58**, 12049–12062 (1998).
- [4] B. Canals and C. Lacroix, “Pyrochlore antiferromagnet: A three-dimensional quantum spin liquid,” *Phys. Rev. Lett.* **80**, 2933–2936 (1998).
- [5] Alexei Kitaev, “Anyons in an exactly solved model and beyond,” *Annals of Physics* **321**, 2–111 (2006).
- [6] M. J. P. Gingras and P. A. McClarty, “Quantum spin ice: a search for gapless quantum spin liquids in pyrochlore magnets,” *Reports on Progress in Physics* **77**, 056501 (2014).
- [7] Lucile Savary and Leon Balents, “Quantum spin liquids: a review,” *Reports on Progress in Physics* **80**, 016502 (2017).
- [8] Takashi Imai and Young S. Lee, “Do quantum spin liquids exist?” *Physics Today* **69**, 30–36 (2016).
- [9] J. Knolle and R. Moessner, “A field guide to spin liquids,” *Annual Review of Condensed Matter Physics* **10**, 451–472 (2019).
- [10] Leon Balents, “Spin liquids in frustrated magnets,” *Nature* **464**, 199–208 (2010).
- [11] Jinsheng Wen, Shun-Li Yu, Shiyan Li, Weiqiang Yu, and Jian-Xin Li, “Experimental identification of quantum spin liquids,” *npj Quantum Materials* **4**, 12 (2019).
- [12] C. Lacroix, P. Mendels, and F. Mila (eds.), *Introduction to Frustrated Magnetism: Materials, Experiments, Theory* (Springer Berlin, 2011).
- [13] M. Udagawa and L. Jaubert (eds.), *Spin Ice* (Springer Cham, 2021).
- [14] Jason S. Gardner, Michel J. P. Gingras, and John E. Greedan, “Magnetic pyrochlore oxides,” *Rev. Mod. Phys.* **82**, 53–107 (2010).
- [15] Alannah M. Hallas, Jonathan Gaudet, and Bruce D. Gaulin, “Experimental insights into ground-state selection of quantum XY pyrochlores,” *Annual Review of Condensed Matter Physics* **9**, 105–124 (2018).
- [16] Jeffrey G. Rau and Michel J.P. Gingras, “Frustrated quantum rare-earth pyrochlores,” *Annual Review of Condensed Matter Physics* **10**, 357–386 (2019).
- [17] Simon Trebst and Ciarán Hickey, “Kitaev materials,” *Physics Reports* **950**, 1–37 (2022).
- [18] H. Takagi, T. Takayama, G. Jackeli, G. Khaliullin, and S. E. Nagler, “Concept and realization of Kitaev quantum spin liquids,” *Nature Reviews Physics* **1**, 264–280 (2019).
- [19] Lucile Savary, Kate A. Ross, Bruce D. Gaulin, Jacob P. C. Ruff, and Leon Balents, “Order by quantum disorder in $\text{Er}_2\text{Ti}_2\text{O}_7$,” *Phys. Rev. Lett.* **109**, 167201 (2012).
- [20] J. Villain, R. Bidaux, J.-P. Carton, and R. Conte, “Order as an effect of disorder,” *J. Phys. France* **41**, 1263–1272 (1980).
- [21] E. F. Shender, “Antiferromagnetic garnets with fluctuonally interacting sublattices,” *Sov. Phys. JETP* **56**, 178 (1982).
- [22] Christopher L. Henley, “Ordering due to disorder in a frustrated vector antiferromagnet,” *Phys. Rev. Lett.* **62**, 2056–2059 (1989).
- [23] Jack R. Tessman, “Magnetic anisotropy at 0°k,” *Phys. Rev.* **96**, 1192–1195 (1954).
- [24] Sona Prakash and Christopher L. Henley, “Ordering due to disorder in dipolar magnets on two-dimensional lattices,” *Phys. Rev. B* **42**, 6574–6589 (1990).
- [25] Kenn Kubo and Tatsuya Kishi, “Ordering due to quantum fluctuations in the frustrated Heisenberg model,” *Journal of the Physical Society of Japan* **60**, 567–572 (1991).
- [26] Andrey Chubukov, “Order from disorder in a kagomé antiferromagnet,” *Phys. Rev. Lett.* **69**, 832–835 (1992).
- [27] Jan N. Reimers and A. J. Berlinsky, “Order by disorder in the classical Heisenberg kagomé antiferromagnet,” *Phys. Rev. B* **48**, 9539–9554 (1993).
- [28] S. T. Bramwell, M. J. P. Gingras, and J. N. Reimers, “Order by disorder in an anisotropic pyrochlore lattice antiferromagnet,” *J. Appl. Phys.* **75**, 5523–5525 (1994).
- [29] Christopher L. Henley, “Selection by quantum fluctuations of dipolar order in a diamond lattice,” *Phys. Rev. Lett.* **73**, 2788–2788 (1994).
- [30] J. D. M. Champion, M. J. Harris, P. C. W. Holdsworth, A. S. Wills, G. Balakrishnan, S. T. Bramwell, E. Čížmár, T. Fennell, J. S. Gardner, J. Lago, D. F. McMorrow, M. Orendáč, A. Orendáčová, D. McK. Paul, R. I. Smith, M. T. F. Telling, and A. Wildes, “ $\text{Er}_2\text{Ti}_2\text{O}_7$: Evidence of quantum order by disorder in a frustrated antiferromagnet,” *Phys. Rev. B* **68**, 020401 (2003).
- [31] G. Baskaran, Diptiman Sen, and R. Shankar, “Spin-S Kitaev model: Classical ground states, order from disorder, and exact correlation functions,” *Phys. Rev. B* **78**, 115116 (2008).
- [32] Paul A. McClarty, Pawel Stasiak, and Michel J. P. Gingras, “Order-by-disorder in the XY pyrochlore antiferromagnet,” *Phys. Rev. B* **89**, 024425 (2014).
- [33] Bimla Danu, Gautam Nambiar, and R. Ganesh, “Extended degeneracy and order by disorder in the square lattice $J_1 - J_2 - J_3$ model,” *Phys. Rev. B* **94**, 094438 (2016).
- [34] Th. Brueckel, B. Dorner, A. G. Gukasov, V. P. Plakhty, W. Prandl, E. F. Shender, and O. P. Smirnov, “Dynamical interaction of antiferromagnetic subsystems: a neutron scattering study of the spinwave spectrum of the garnet $\text{Fe}_2\text{Ca}_3(\text{GeO}_4)_3$,” *Zeitschrift für Physik B Condensed Matter* **72**, 477–485 (1988).
- [35] Y. J. Kim, A. Aharony, R. J. Birgeneau, F. C. Chou, O. Entin-Wohlman, R. W. Erwin, M. Greven, A. B. Harris, M. A. Kast-

- ner, I. Ya. Korenblit, Y. S. Lee, and G. Shirane, “Ordering due to quantum fluctuations in $\text{Sr}_2\text{Cu}_3\text{O}_4\text{Cl}_2$,” *Phys. Rev. Lett.* **83**, 852–855 (1999).
- [36] K. A. Ross, Y. Qiu, J. R. D. Copley, H. A. Dabkowska, and B. D. Gaulin, “Order by disorder spin wave gap in the XY pyrochlore magnet $\text{Er}_2\text{Ti}_2\text{O}_7$,” *Phys. Rev. Lett.* **112**, 057201 (2014).
- [37] C. L. Sarkis, J. G. Rau, L. D. Sanjeeva, M. Powell, J. Kolis, J. Marbey, S. Hill, J. A. Rodriguez-Rivera, H. S. Nair, D. R. Yahne, S. Säubert, M. J. P. Gingras, and K. A. Ross, “Unravelling competing microscopic interactions at a phase boundary: A single-crystal study of the metastable antiferromagnetic pyrochlore $\text{Yb}_2\text{Ge}_2\text{O}_7$,” *Phys. Rev. B* **102**, 134418 (2020).
- [38] N. W. Ashcroft and N. D. Mermin, *Solid State Physics* (Saunders College Publishing, Fort Worth, 1976).
- [39] Xiao-Gang Wen, *Quantum Field Theory of Many-Body Systems: From the Origin of Sound to an Origin of Light and Electrons* (Oxford University Press, 2007).
- [40] P. A. McClarty, S. H. Curnoe, and M. J. P. Gingras, “Energetic selection of ordered states in a model of the $\text{Er}_2\text{Ti}_2\text{O}_7$ frustrated pyrochlore XY antiferromagnet,” *Journal of Physics: Conference Series* **145**, 012032 (2009).
- [41] Sylvain Petit, Julien Robert, Solène Guitteny, Pierre Bonville, Claudia Decorse, Jacques Ollivier, Hannu Mutka, Michel J. P. Gingras, and Isabelle Mirebeau, “Order by disorder or energetic selection of the ground state in the XY pyrochlore antiferromagnet $\text{Er}_2\text{Ti}_2\text{O}_7$: An inelastic neutron scattering study,” *Phys. Rev. B* **90**, 060410 (2014).
- [42] Jeffrey G. Rau, Sylvain Petit, and Michel J. P. Gingras, “Order by virtual crystal field fluctuations in pyrochlore XY antiferromagnets,” *Phys. Rev. B* **93**, 184408 (2016).
- [43] The lower intensity at the band minimum compared to its vicinity is a numerical artifact. Due to the finite frequency resolution of the spin-dynamics simulations, the intensity maximum of the PG mode may have fallen between frequency grid points, resulting in an (apparent) lower intensity at the band minimum.
- [44] Steven Weinberg, “Approximate symmetries and pseudo-Goldstone bosons,” *Phys. Rev. Lett.* **29**, 1698–1701 (1972).
- [45] C.P. Burgess, “Goldstone and pseudo-Goldstone bosons in nuclear, particle and condensed-matter physics,” *Physics Reports* **330**, 193–261 (2000).
- [46] Muneto Nitta and Daisuke A. Takahashi, “Quasi-Nambu-Goldstone modes in nonrelativistic systems,” *Phys. Rev. D* **91**, 025018 (2015).
- [47] Zohar Nussinov and Jeroen van den Brink, “Compass models: Theory and physical motivations,” *Rev. Mod. Phys.* **87**, 1–59 (2015).
- [48] Julien Dorier, Federico Becca, and Frédéric Mila, “Quantum compass model on the square lattice,” *Phys. Rev. B* **72**, 024448 (2005).
- [49] G. Jackeli and G. Khaliullin, “Mott insulators in the strong spin-orbit coupling limit: From Heisenberg to a quantum compass and Kitaev models,” *Phys. Rev. Lett.* **102**, 017205 (2009).
- [50] F. Trouselet, A. M. Oleś, and P. Horsch, “Compass-Heisenberg model on the square lattice —spin order and elementary excitations,” *Europhysics Letters* **91**, 40005 (2010).
- [51] Fabien Trouselet, Andrzej M. Oleś, and Peter Horsch, “Magnetic properties of nanoscale compass-Heisenberg planar clusters,” *Phys. Rev. B* **86**, 134412 (2012).
- [52] S. Boseggia, R. Springell, H. C. Walker, H. M. Rønnow, Ch. Rüegg, H. Okabe, M. Isobe, R. S. Perry, S. P. Collins, and D. F. McMorrow, “Robustness of basal-plane antiferromagnetic order and the $J_{\text{eff}}=1/2$ state in single-layer iridate spin-orbit Mott insulators,” *Phys. Rev. Lett.* **110**, 117207 (2013).
- [53] Vamshi M. Katukuri, Viktor Yushankhai, Liudmila Siurakshina, Jeroen van den Brink, Liviu Hozoi, and Ioannis Rousochatzakis, “Mechanism of basal-plane antiferromagnetism in the spin-orbit driven iridate Ba_2IrO_4 ,” *Phys. Rev. X* **4**, 021051 (2014).
- [54] Artem A. Vladimirov, Dieter Ihle, and Nikolay M. Plakida, “Magnetic order in the two-dimensional compass-Heisenberg model,” *Eur. Phys. J. B* **88**, 148 (2015).
- [55] Long Zhang, Fa Wang, and Dung-Hai Lee, “Compass impurity model of Tb substitution in Sr_2IrO_4 ,” *Phys. Rev. B* **94**, 161118 (2016).
- [56] Haruki Watanabe, “Counting rules of Nambu–Goldstone modes,” *Annual Review of Condensed Matter Physics* **11**, 169–187 (2020).
- [57] Sidney Coleman, “There are no Goldstone bosons in two dimensions,” *Communications in Mathematical Physics* **31**, 259–264 (1973).
- [58] N. D. Mermin and H. Wagner, “Absence of ferromagnetism or antiferromagnetism in one- or two-dimensional isotropic Heisenberg models,” *Phys. Rev. Lett.* **17**, 1133–1136 (1966).
- [59] P. C. Hohenberg, “Existence of long-range order in one and two dimensions,” *Phys. Rev.* **158**, 383–386 (1967).
- [60] See Supplemental Material at (...) for details about Monte Carlo and spin-dynamics simulations and finite size scaling analysis, as well as details of the linear and non-linear spin wave theory, including of cancellation of divergences in the PG gap calculation and derivation of logarithmic correction to the magnetization. It also includes Refs. [62, 66, 67, 70–72, 89–97].
- [61] L. Landau and E. Lifshitz, “3 - On the theory of the dispersion of magnetic permeability in ferromagnetic bodies,” in *Perspectives in Theoretical Physics*, edited by L. P. Pitaevski (Pergamon, Amsterdam, 1992) pp. 51–65, reprinted from *Physikalische Zeitschrift der Sowjetunion* 8, Part 2, 153, 1935.
- [62] A. Auerbach, *Interacting Electrons and Quantum Magnetism*, Graduate Texts in Contemporary Physics (Springer New York, 1998).
- [63] P. C. Martin, E. D. Siggia, and H. A. Rose, “Statistical dynamics of classical systems,” *Phys. Rev. A* **8**, 423–437 (1973).
- [64] Uli Dekker and Fritz Haake, “Fluctuation-dissipation theorems for classical processes,” *Phys. Rev. A* **11**, 2043–2056 (1975).
- [65] C. P. Enz and L. Garrido, “Perturbation theory for classical thermodynamic Green’s functions,” *Phys. Rev. A* **14**, 1258–1268 (1976).
- [66] H. Bruus and K. Flensberg, *Many-Body Quantum Theory in Condensed Matter Physics: An Introduction*, Oxford Graduate Texts (Oxford University Press, Oxford, 2004).
- [67] J.P. Blaizot and G. Ripka, *Quantum Theory of Finite Systems* (MIT Press, Cambridge, 1986).
- [68] G. D. Mahan, *Many Particle Physics, Third Edition* (Springer New York, 2000).
- [69] Mehran Kardar, *Statistical Physics of Particles* (Cambridge University Press, 2007).
- [70] P. D. Loly, “The Heisenberg ferromagnet in the selfconsistently renormalized spin wave approximation,” *Journal of Physics C: Solid State Physics* **4**, 1365–1377 (1971).
- [71] A. V. Chubukov, S. Sachdev, and T. Senthil, “Large- S expansion for quantum antiferromagnets on a triangular lattice,” *Journal of Physics: Condensed Matter* **6**, 8891–8902 (1994).
- [72] Jeffrey G. Rau, Paul A. McClarty, and Roderich Moessner, “Pseudo-Goldstone gaps and order-by-quantum disorder in frustrated magnets,” *Phys. Rev. Lett.* **121**, 237201 (2018).
- [73] H. Goldstein, C. P. Poole, and J. L. Safko, *Classical Mechanics, Third Edition* (Pearson, 2002).
- [74] Subhankar Khatua, Michel J. P. Gingras, and Jeffrey G. Rau, (unpublished).

- [75] E. Lhotel, J. Robert, E. Ressouche, F. Damay, I. Mirebeau, J. Ollivier, H. Mutka, P. Dalmas de Réotier, A. Yaouanc, C. Marin, C. Decorse, and S. Petit, “Field-induced phase diagram of the XY pyrochlore antiferromagnet $\text{Er}_2\text{Ti}_2\text{O}_7$,” *Phys. Rev. B* **95**, 134426 (2017).
- [76] Cheng Gong, Lin Li, Zhenglu Li, Huiwen Ji, Alex Stern, Yang Xia, Ting Cao, Wei Bao, Chenzhe Wang, Yuan Wang, Z. Q. Qiu, R. J. Cava, Steven G. Louie, Jing Xia, and Xiang Zhang, “Discovery of intrinsic ferromagnetism in two-dimensional van der Waals crystals,” *Nature* **546**, 265–269 (2017).
- [77] Lebing Chen, Jae-Ho Chung, Matthew B. Stone, Alexander I. Kolesnikov, Barry Winn, V. Ovidiu Garlea, Douglas L. Abernathy, Bin Gao, Mathias Augustin, Elton J. G. Santos, and Pengcheng Dai, “Magnetic field effect on topological spin excitations in CrI_3 ,” *Phys. Rev. X* **11**, 031047 (2021).
- [78] S. E. Nikitin, B. Fåk, K. W. Krämer, T. Fennell, B. Normand, A. M. Läuchli, and Ch. Rüegg, “Thermal evolution of Dirac magnons in the honeycomb ferromagnet CrBr_3 ,” *Phys. Rev. Lett.* **129**, 127201 (2022).
- [79] Yilong Han, Yair Shokef, Ahmed M. Alsayed, Peter Yunker, Tom C. Lubensky, and Arjun G. Yodh, “Geometric frustration in buckled colloidal monolayers,” *Nature* **456**, 898–903 (2008).
- [80] Yair Shokef, Anton Souslov, and T. C. Lubensky, “Order by disorder in the antiferromagnetic Ising model on an elastic triangular lattice,” *Proceedings of the National Academy of Sciences* **108**, 11804–11809 (2011).
- [81] Jerzy Cioslowski and Asiri Nanayakkara, “Endohedral fullerenes: A new class of ferroelectric materials,” *Phys. Rev. Lett.* **69**, 2871–2873 (1992).
- [82] Shinobu Aoyagi, Norihisa Hoshino, Tomoyuki Akutagawa, Yuki Sado, Ryo Kitaura, Hisanori Shinohara, Kunihisa Sugimoto, Rui Zhang, and Yasujiro Murata, “A cubic dipole lattice of water molecules trapped inside carbon cages,” *Chemical Communications* **50**, 524–526 (2014).
- [83] B. P. Gorshunov, V. I. Torgashev, E. S. Zhukova, V. G. Thomas, M. A. Belyanchikov, C. Kadlec, F. Kadlec, M. Savinov, T. Ostapchuk, J. Petzelt, J. Prokleška, P. V. Tomas, E. V. Pestrjakov, D. A. Fursenko, G. S. Shakurov, A. S. Prokhorov, V. S. Gorelik, L. S. Kadyrov, V. V. Uskov, R. K. Kremer, and M. Dressel, “Incipient ferroelectricity of water molecules confined to nano-channels of beryl,” *Nature Communications* **7**, 12842 (2016).
- [84] M. A. Belyanchikov, M. Savinov, Z. V. Bedran, P. Bednyakov, P. Proschek, J. Prokleska, V. A. Abalmasov, J. Petzelt, E. S. Zhukova, V. G. Thomas, A. Dudka, A. Zhugayevych, A. S. Prokhorov, V. B. Anzin, R. K. Kremer, J. K. H. Fischer, P. Lunkenheimer, A. Loidl, E. Uykur, M. Dressel, and B. Gorshunov, “Dielectric ordering of water molecules arranged in a dipolar lattice,” *Nature Communications* **11**, 3927 (2020).
- [85] Oleksandr V. Dobrovolskiy, Oleksandr V. Pylypovskiy, Luka Skoric, Amalio Fernández-Pacheco, Arjen Van Den Berg, Sam Ladak, and Michael Huth, “Complex-shaped 3D nanoarchitectures for magnetism and superconductivity,” in *Curvilinear Micromagnetism: From Fundamentals to Applications*, edited by Denys Makarov and Denis D. Sheka (Springer International Publishing, Cham, 2022) pp. 215–268.
- [86] Lukas Keller, Mohanad K. I. Al Mamoori, Jonathan Pieper, Christian Gspan, Irina Stockem, Christian Schröder, Sven Barth, Robert Winkler, Harald Plank, Merlin Pohlit, Jens Müller, and Michael Huth, “Direct-write of free-form building blocks for artificial magnetic 3D lattices,” *Scientific Reports* **8**, 6160 (2018).
- [87] Andrew May, Matthew Hunt, Arjen Van Den Berg, Alaa Hejazi, and Sam Ladak, “Realisation of a frustrated 3D magnetic nanowire lattice,” *Communications Physics* **2**, 13 (2019).
- [88] Peter Fischer, Dédalo Sanz-Hernández, Robert Streubel, and Amalio Fernández-Pacheco, “Launching a new dimension with 3D magnetic nanostructures,” *APL Materials* **8**, 010701 (2020).
- [89] J. D. Alzate-Cardona, D. Sabogal-Suárez, R. F. L. Evans, and E. Restrepo-Parra, “Optimal phase space sampling for Monte Carlo simulations of Heisenberg spin systems,” *Journal of Physics: Condensed Matter* **31**, 095802 (2019).
- [90] Michael Creutz, “Overrelaxation and Monte Carlo simulation,” *Phys. Rev. D* **36**, 515–519 (1987).
- [91] M. E. J. Newman and G. T. Barkema, *Monte Carlo methods in statistical physics* (Clarendon Press, Oxford, 1999).
- [92] J. R. Dormand and P. J. Prince, “A family of embedded Runge-Kutta formulae,” *Journal of Computational and Applied Mathematics* **6**, 19–26 (1980).
- [93] K. Ahnert and M. Mulansky, “Odeint – solving ordinary differential equations in C++,” *AIP Conference Proceedings* **1389**, 1586–1589 (2011).
- [94] K. Ahnert and M. Mulansky, “Boost C++ Library: Odeint,” (2012).
- [95] J. C. Bowman and M. Roberts, “FFTW++: A fast Fourier transform C++ header class for the FFTW3 library,” (2010).
- [96] M. E. Zhitomirsky and A. L. Chernyshev, “Colloquium: Spontaneous magnon decays,” *Rev. Mod. Phys.* **85**, 219–242 (2013).
- [97] P. M. Chaikin and T. C. Lubensky, *Principles of Condensed Matter Physics* (Cambridge University Press, 1995).

Supplemental Material for “Pseudo-Goldstone modes and dynamical gap generation from order-by-thermal-disorder”

Subhankar Khatua,^{1,2} Michel J. P. Gingras,² and Jeffrey G. Rau¹

¹Department of Physics, University of Windsor, 401 Sunset Avenue, Windsor, Ontario, N9B 3P4, Canada

²Department of Physics and Astronomy, University of Waterloo, Waterloo, Ontario, N2L 3G1, Canada

(Dated: January 27, 2023)

I. DETAILS OF MONTE CARLO SIMULATIONS

A. Details of Monte Carlo procedure

The Monte Carlo (MC) simulations described in the main text are based on adaptive single-site Metropolis moves [1], combined with over-relaxation moves [2]. A typical single-site Metropolis move involves randomly selecting a spin and changing its orientation to a random direction. However, at low temperature, most such moves result in configurations that are of much higher energies and thus rejected [3]. Therefore, we follow an adaptive approach that selects a spin randomly and changes its orientation to a Gaussian distributed random direction *within a solid-angle of certain width*. The solid-angle-width changes adaptively to ensure that the update-acceptance rate remains close to 50% at each temperature (see Ref. [1] for details). The over-relaxation move rotates a randomly selected spin by a random angle about its local exchange field. This move is energy-conserving and thus always accepted. We define a Monte Carlo sweep at a certain temperature as a combination of N (total number of spins) random successive adaptive single-site Metropolis moves with each followed by five random over-relaxation moves. All the simulation results discussed in the main text have been obtained by considering periodic boundary conditions on the square lattice of size L by L and $N = L^2$ spins. As in the main text, we use units such that $J = \hbar = k_B = 1$.

B. Simulation details of the order parameter distribution

Starting from a random spin configuration at high temperature, $T = 10$ (larger than K) where the system is in the paramagnetic phase, we slowly cool down in steps of size $\delta T = 0.1$ to a final temperature $T = 0.4$ (much smaller than K). At each temperature, we perform 10^5 MC sweeps to equilibrate the system. Finally, at $T = 0.4$, after equilibration, we record the net magnetization-per-spin over 10^6 MC samples, leaving five MC sweeps in between two consecutive measurements. From the net magnetization per spin, $\mathbf{M} = (M_x, M_y, M_z)$, we calculate $\phi = \arctan(M_y/M_x)$, computing a distribution for ϕ . Since the ferromagnetic Heisenberg-compass model has a C_4 rotation symmetry in the \hat{x} - \hat{y} plane, we symmetrize the distribution by shifting the data by $\pi/2$, π , and $3\pi/2$, i.e., add $\pi/2$, π , and $3\pi/2$ to each entry of the dataset. We have plotted the final dataset as a probability density, $P(\phi)$ for $\phi \in [-\pi/4, \pi/4]$ with 50 bins for three different system sizes, $N = 6^2, 10^2$, and 14^2 in Fig. 1(a) in the main text. We have chosen a large

value for K , i.e., $K = 5$, for all simulations in order to obtain a strong selection effect at accessible system sizes. For the gross spectral features, the largest system size considered for spin-dynamics simulations was $N = 100^2$, while for detailed features, such as the temperature dependence of the pseudo-Goldstone (PG) gap, up to $N = 40^2$ was used. Had smaller values of K been used, all the MC simulations, as well as spin-dynamics simulations, would have had to be performed for much larger system sizes to obtain results that converge when system size is extrapolated to the thermodynamic limit ($N \rightarrow \infty$).

C. Simulation details of magnetization and its derivative with respect to temperature

Independently at each temperature T , 5×10^5 MC sweeps are performed on a perfectly aligned ferromagnetic spin configuration along \hat{x} for equilibration, followed by 3×10^6 successive MC sweeps to measure the net magnetization along \hat{x} (M), energy (E), and their product (EM). Their product is recorded in order to calculate the derivative of the magnetization with respect to temperature, given by

$$\frac{\partial M}{\partial T} \equiv \frac{\langle EM \rangle - \langle E \rangle \langle M \rangle}{T^2}, \quad (\text{S1})$$

where $\langle x \rangle$ is the MC thermal average of quantity x . To estimate the statistical errors on static quantities, the 3×10^6 measurements are divided into 30 blocks, and then resampled using the standard bootstrap method [3]. Typically, $O(10^3)$ bootstrap samples were generated from these blocks to estimate the statistical errors. In Fig. 3 of the main text, the error bars shown correspond to twice the standard deviation estimated via bootstrap.

II. DETAILS OF SPIN-DYNAMICS SIMULATIONS

Numerical integrations of the Landau-Lifshitz equations have been done using an adaptive step size RK5(4) Dormand-Prince integrator [4] from the Boost-Odeint C++ library [5, 6]. The initial spin configurations for the numerical integration are generated from MC simulations described in Sec. I.

To obtain the results shown in Fig. 1(b) in the main text, we perform 5×10^5 equilibration MC sweeps on a perfectly aligned ferromagnetic configuration along \hat{x} at $T = 0.4$. Starting from the final state, we perform another 15×10^3 MC sweeps for 350 independent parallel runs to generate well-equilibrated configurations at $T = 0.4$. Next, we feed each

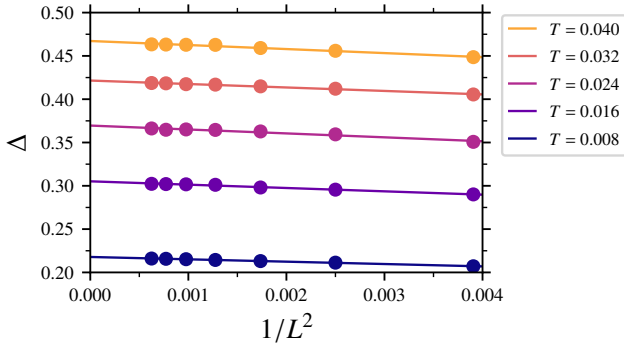


FIG. S1. Finite size scaling of the PG gap obtained from spin-dynamics simulations for several temperatures ($K = 5$).

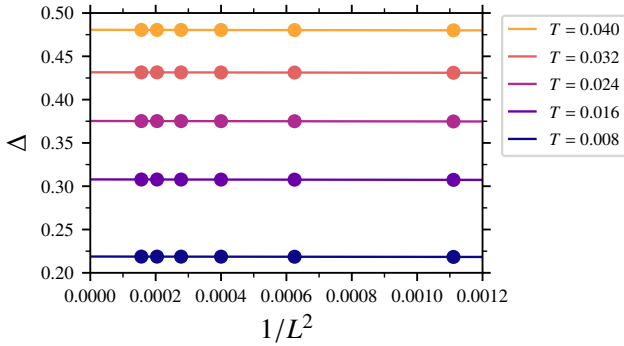


FIG. S2. Finite size scaling of the PG gap obtained using SCMFT for several temperatures ($K = 5$).

of these 350 configurations into the Dormand-Prince integrator as an initial state and integrate to a final time, $t_{\max} = 50$. The error tolerance of the integrator is set to 10^{-8} , such that the energy-per-spin and individual spin lengths are conserved to at least one part in 10^7 and 10^{10} , respectively. In each of these independent 350 integrations, we calculate the Fourier transform of the spin configurations in space and time, $\mathcal{S}(\mathbf{k}, \omega)$ using FFTW++ [7] and then compute the dynamical structure

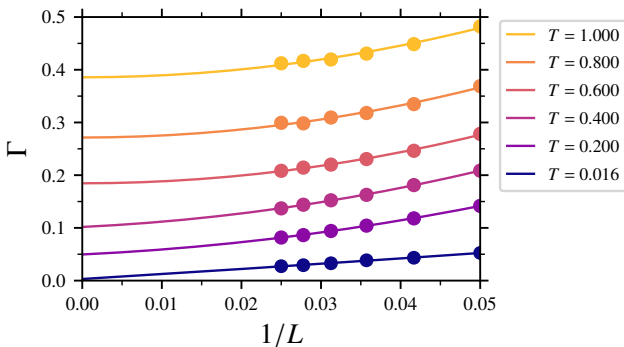


FIG. S3. Finite size scaling of the PG linewidth obtained from spin-dynamics simulations for several temperatures ($K = 5$).

factor, $\mathcal{S}(\mathbf{k}, \omega) = |\mathcal{S}(\mathbf{k}, \omega)|^2$, finally taking an average of the structure factors found from the 350 initial configurations to obtain Fig. 1(b).

The results in Fig. 1(c) in the main text are obtained as follows: The system is initialized in a perfectly aligned ferromagnetic configuration along \hat{x} at $T = 0.0004$, and slowly warmed up in steps of $\delta T = 0.0004$ to a temperature $T = 0.04$. At each temperature, we perform 10^5 equilibration MC sweeps, generating a configuration at $T = 0.008, 0.016, 0.024, 0.032, 0.04$. At each of these temperatures, we then apply the following procedure. Starting from a given spin configuration, say at $T = 0.008$, we generate a total of 2×10^3 configurations independently by performing 10^5 MC sweeps. Each of these configurations is fed into the Dormand-Prince integrator independently to integrate to a final time, $t_{\max} = 2500$. Note that t_{\max} here is taken to be much larger than the $t_{\max} = 50$ value used to obtain the results shown in Fig. 1(b). As discussed in the main text, to determine the PG gap, Δ , and linewidth, Γ , a much higher frequency resolution is needed and thus the total integration time must be larger. The error tolerance of the integrator is set to 10^{-10} , such that the energy-per-spin and spin-length are conserved to at least one part in 10^8 and 10^{10} , respectively. After the time evolution, we compute the Fourier transform of the spin configurations in space and time using FFTW++ and then compute the dynamical structure factor, $\mathcal{S}(\mathbf{k}, \omega)$. Finally, we perform an average over the 2×10^3 initial spin configurations to obtain the average dynamical structure factor at $T = 0.008$. In Fig. 1(c), we show only a cut of the average dynamical structure factor at the zone center, $\mathcal{S}(\mathbf{0}, \omega)$. To clearly visualize $\mathcal{S}(\mathbf{0}, \omega)$ at several different temperatures in a single plot, we stagger them on the y -axis with a constant spacing between the $\mathcal{S}(\mathbf{0}, \omega)$ data at two consecutive temperatures.

To obtain the results shown in Fig. 2 of the main text, we proceed as follows: At each temperature, we follow the same method as described for Fig. 1(c) in the previous paragraph and compute $\mathcal{S}(\mathbf{0}, \omega)$ for several system sizes, $L = 20, 24, 28, 32, 36$, and 40 . To find the gap and linewidth for each system size, we fit each data to a Gaussian (a Gaussian lineshape fits the data in the range $T \leq 0.04$ best, compared to, e.g., a Lorentzian). The center of the Gaussian is used to define the PG gap and the full-width at half maximum (FWHM) of the Gaussian, i.e., 2.355σ (standard deviation), is taken as the PG linewidth. Then, finite size L -dependent PG gaps and linewidths are then extrapolated in system size ($L \rightarrow \infty$) to obtain the corresponding values in the thermodynamic limit. Finite size scaling of the PG gap is shown in Fig. S1. The finite size scaling of the PG gap obtained using the self-consistent mean-field theory (SCMFT) is shown in Fig. S2 (See Sec. III E for details).

At very low temperatures, e.g., $T \leq 0.04$, where $\mathcal{S}(\mathbf{0}, \omega)$ falls very sharply away from the center of the peak, a Gaussian lineshape is a natural choice. However, as temperature increases further, $\mathcal{S}(\mathbf{0}, \omega)$ shows more pronounced tails and a Lorentzian lineshape was found to provide a better description of the data. Finite size scaling of the PG linewidth is shown in Fig. S3. At $T = 0.016$, the PG linewidths for different system sizes are found by fitting to a Gaussian while for

the remaining temperatures in Fig. S3, the PG linewidths are found from fitting to Lorentzian (via the FWHM of the corresponding Lorentzian). Finite size scaling reveals that at very low temperatures, the PG linewidth scales almost linearly with $1/L$ with the scaling becoming quadratic in $1/L$ as temperature increases (see Fig. S3).

III. SPIN WAVE THEORY

Here, we elaborate on the formalism for interacting spin waves in the ferromagnetic Heisenberg-compass model on the square lattice. We consider the Heisenberg-compass model Hamiltonian

$$\mathcal{H} = - \sum_{r\delta} [JS_r \cdot S_{r+\delta} + KS_r^\delta S_{r+\delta}^\delta] \equiv \sum_{r\delta} S_r^\top J_\delta S_{r+\delta}, \quad (\text{S2})$$

where $\delta = \hat{x}, \hat{y}$ denotes the nearest-neighbour (horizontal and vertical) bond directions. For $J > 0$ and $K > 0$, the classical ground state is ferromagnetic and has an accidental degeneracy parametrized by an angle ϕ

$$S_r = S(\cos \phi \hat{x} + \sin \phi \hat{y}). \quad (\text{S3})$$

For small $|K|$ and $K < 0$, one finds only a (symmetry-enforced) discrete degeneracy, with $S_r = \pm S \hat{z}$. For large $|K|$ and $K < 0$, the ground state is described by an XY -stripe phase parametrized by a single angle whose two extreme limits are X -stripe phase (i.e., all spins are lying along the \hat{x} axis, arranging themselves antiferromagnetically along the \hat{x} axis and ferromagnetically along the \hat{y} axis) and Y -stripe phase (i.e., all spins are lying along the \hat{y} axis, arranging themselves antiferromagnetically along the \hat{y} axis and ferromagnetically along the \hat{x} axis). The phases for $J < 0$ can be obtained by mapping $S_r \rightarrow (-1)^r S_r$ which alternates on the two sublattices. We note that the dynamics however differ between $J > 0$ and $J < 0$, since the sign change on one sublattice is not a canonical transformation.

Returning to the $J > 0, K > 0$ case, we define a frame aligned with the ground state with angle ϕ

$$\hat{e}_x = -\sin \phi \hat{x} + \cos \phi \hat{y}, \quad \hat{e}_y = \hat{z}, \quad \hat{e}_z = \cos \phi \hat{x} + \sin \phi \hat{y},$$

as well as $\hat{e}_\pm \equiv (\hat{e}_x \pm i\hat{e}_y)/\sqrt{2}$ and $\hat{e}_0 \equiv \hat{e}_z$. We then have the local exchanges $\mathcal{J}_\delta^{\mu\nu} = \hat{e}_\mu^\top J_\delta \hat{e}_\nu$. The Fourier transforms of the exchange matrices, $\mathcal{J}_\delta^{\mu\nu}$, are defined as $\mathcal{J}_k \equiv \sum_\delta 2 \cos(\mathbf{k} \cdot \delta) \mathcal{J}_\delta$ where the fact that $-\delta$ and δ are equivalent has been used. Explicitly, these are given by

$$\begin{aligned} \mathcal{J}_k^{+-} &= -(2J + K \sin^2 \phi) \cos k_x - (2J + K \cos^2 \phi) \cos k_y, \\ \mathcal{J}_k^{00} &= -2(J + K \cos^2 \phi) \cos k_x - 2(J + K \sin^2 \phi) \cos k_y, \\ \mathcal{J}_k^{++} &= -(K \sin^2 \phi) \cos k_x - (K \cos^2 \phi) \cos k_y, \\ \mathcal{J}_k^{0\pm} &= -\frac{K}{\sqrt{2}} \sin(2\phi) (\cos k_y - \cos k_x), \end{aligned}$$

with $\mathcal{J}_k^{-+} = [\mathcal{J}_k^{+-}]^*$, $\mathcal{J}_k^{--} = [\mathcal{J}_k^{++}]^*$ and $\mathcal{J}_k^{0\pm} = \mathcal{J}_k^{\pm 0}$. Note that $\mathcal{J}_0^{00} = -2(2J + K)$. For one of the four ground states

selected by order-by-thermal-disorder (ObTD), e.g. $\phi = 0$, these $\mathcal{J}_k^{\mu\nu}$ are given by

$$\begin{aligned} \mathcal{J}_k^{+-} &= -2J \cos k_x - (2J + K) \cos k_y, \\ \mathcal{J}_k^{00} &= -2(J + K) \cos k_x - 2J \cos k_y, \\ \mathcal{J}_k^{++} &= -K \cos k_y, \end{aligned}$$

where $\mathcal{J}_k^{0\pm} = 0$. Performing the usual Holstein-Primakoff expansion [8] to $O(S^0)$ on this model yields [9]

$$\mathcal{H} \approx E_0 + \mathcal{H}_2 + (\mathcal{H}_{4,2-2} + \mathcal{H}_{4,3-1} + \mathcal{H}_{4,1-3}) + \dots, \quad (\text{S4})$$

where we have defined the constant classical part $E_0 = -NS^2(2J + K)$ [at $O(S^2)$] and

$$\mathcal{H}_2 = \sum_k \left[A_k a_k^\dagger a_k + \frac{1}{2!} (B_k a_k^\dagger a_{-k}^\dagger + B_k^* a_{-k} a_k) \right], \quad (\text{S5a})$$

$$\mathcal{H}_{4,2-2} = \frac{1}{N} \sum_{kk'q} \frac{1}{(2!)^2} V_{k,k',q} a_{k+q}^\dagger a_{k'-q}^\dagger a_{k'} a_k, \quad (\text{S5b})$$

$$\mathcal{H}_{4,3-1} = \frac{1}{N} \sum_{kk'q} \frac{1}{3!} D_{k,k',q} a_{k'}^\dagger a_q^\dagger a_{k+k'+q}^\dagger = \mathcal{H}_{4,1-3}^\dagger, \quad (\text{S5c})$$

This includes the quadratic parts [at $O(S)$] in \mathcal{H}_2 as well as the quartic parts [at $O(S^0)$] in $\mathcal{H}_4 \equiv \mathcal{H}_{4,2-2} + \mathcal{H}_{4,3-1} + \mathcal{H}_{4,1-3}$. The quartic part has been decomposed into a $2-2$ scattering term, $\mathcal{H}_{4,2-2}$, and anomalous $3-1$ and $1-3$ terms, $\mathcal{H}_{4,3-1}$ and $\mathcal{H}_{4,1-3}$. Since $\mathcal{J}_k^{0,\pm} = 0$, there are no three boson terms in \mathcal{H} [Eq. (S4)]. In terms of the local exchanges, the coefficients in \mathcal{H}_2 and \mathcal{H}_4 are given explicitly by

$$\begin{aligned} A_k &= S(\mathcal{J}_k^{+-} - \mathcal{J}_0^{00}), \\ B_k &= S\mathcal{J}_k^{++}, \\ V_{k,k',q} &= \frac{1}{2} (\mathcal{J}_{k'-k-q}^{00} + \mathcal{J}_{-q}^{00} + \mathcal{J}_{+q}^{00} + \mathcal{J}_{k-k'+q}^{00}) \\ &\quad - \frac{1}{2} (\mathcal{J}_k^{+-} + \mathcal{J}_{k'}^{+-} + \mathcal{J}_{k'-q}^{+-} + \mathcal{J}_{k+q}^{+-}), \\ D_{k,k',q} &= -\frac{1}{2} (\mathcal{J}_k^{++} + \mathcal{J}_{k'}^{++} + \mathcal{J}_q^{++}). \end{aligned}$$

By construction, these coefficients must satisfy the symmetry relations

$$\begin{aligned} A_k &= A_k^*, \\ B_k &= B_{-k}, \\ V_{k,k',q} &= V_{k',k,-q} = V_{k,k',k'-k-q} = V_{k',k,k-k'+q} = V_{k+q,k'-q,-q}^*, \\ D_{k,k',q} &= D_{k,q,k'} = D_{k',k,q} = D_{k',q,k} = D_{q,k,k'} = D_{q,k',k}. \end{aligned}$$

A. Non-Interacting Spin-Waves

Consider first only the quadratic (non-interacting magnon) portion of \mathcal{H} ,

$$\mathcal{H}_2 = \sum_k \left[A_k a_k^\dagger a_k + \frac{1}{2!} (B_k a_k^\dagger a_{-k}^\dagger + \text{H.c.}) \right]. \quad (\text{S6})$$

This can be diagonalized by the usual Bogoliubov transformation [8]. Defining the matrix

$$\mathbf{M}_k \equiv \begin{pmatrix} A_k & B_k \\ B_k^* & A_k \end{pmatrix}, \quad (\text{S7})$$

the spin-wave spectrum is obtained by diagonalization of $\sigma_z \mathbf{M}_k$, where σ_z is a (block) Pauli matrix. One finds the positive frequency mode

$$\omega_k = \sqrt{A_k^2 - |B_k|^2} > 0.$$

For the ferromagnetic Heisenberg-compass model, A_k and B_k are given by

$$A_k = -S \left[(2J + K \sin^2 \phi) \cos k_x + (2J + K \cos^2 \phi) \cos k_y - 2(2J + K) \right]$$

$$B_k = -S \left[(K \sin^2 \phi) \cos k_x + (K \cos^2 \phi) \cos k_y \right].$$

Note that $A_0 = KS$ and $B_0 = -KS$, yielding a zero energy mode at $\mathbf{k} = \mathbf{0}$, with $\omega_0 = 0$ and with both A_k and B_k real. The eigenvector of $\sigma_z \mathbf{M}_k$ associated with the positive mode can be written as (u_k, v_k) where

$$u_k = \sqrt{\frac{\omega_k + A_k}{2\omega_k}}, \quad v_k = -\frac{B_k}{\sqrt{2\omega_k(\omega_k + A_k)}},$$

which we have defined so that $u_k^2 - v_k^2 = 1$. Note that since both A_k and B_k are inversion even, we have $u_{-k} = u_k$, $v_{-k} = v_k$ and $\omega_k = \omega_{-k}$. Since both A_k and B_k are real, we find that u_k and v_k are real as well. The diagonalized boson operators are defined via

$$a_k = u_k \gamma_k + v_k \gamma_{-k}^\dagger, \quad a_k^\dagger = v_k \gamma_{-k} + u_k \gamma_k^\dagger.$$

Expectation values of bilinears of these bosons can be written in terms of u_k and v_k . Noting that at temperature T these are

$$\langle \gamma_k^\dagger \gamma_k \rangle = n_B(\omega_k), \quad \langle \gamma_k \gamma_{-k}^\dagger \rangle = 1 + n_B(\omega_k),$$

where $n_B(\omega) = [\exp(\omega/T) - 1]^{-1}$ is the boson thermal occupation number. The above thermal expectations for the original a -bosons are given by

$$\langle a_k^\dagger a_k \rangle = n_B(\omega_k) u_k^2 + [1 + n_B(\omega_k)] v_k^2,$$

$$\langle a_k a_{-k} \rangle = \langle a_{-k}^\dagger a_k^\dagger \rangle^* = [1 + 2n_B(\omega_k)] u_k v_k.$$

In the classical limit, where $T \gg \omega_k$, we have $n_B(\omega_k) \approx T/\omega_k \gg 1$. The expectations then become

$$\langle a_k^\dagger a_k \rangle = \frac{T}{\omega_k} (u_k^2 + v_k^2) = \frac{T}{\omega_k} \left(\frac{A_k}{\omega_k} \right), \quad (\text{S8a})$$

$$\langle a_k a_{-k} \rangle = \langle a_{-k}^\dagger a_k^\dagger \rangle = \frac{2T}{\omega_k} u_k v_k = -\frac{T}{\omega_k} \left(\frac{B_k}{\omega_k} \right). \quad (\text{S8b})$$

Finally, the ordered moment (selected by ObTD), $\mathbf{M} \equiv \frac{1}{N} \sum_r \langle \mathbf{S}_r \rangle \equiv M \hat{\mathbf{x}}$, can be expressed in terms of these boson averages as

$$M = S - \frac{1}{N} \sum_k \langle a_k^\dagger a_k \rangle \equiv S \left(1 - \frac{T}{SN} \sum_k \frac{A_k}{\omega_k^2} \right). \quad (\text{S9})$$

B. Interacting Spin-Waves

To consider the effects of the quartic parts of \mathcal{H} in Eq. S4, $\mathcal{H}_{4,2-2}$, $\mathcal{H}_{4,3-1}$ and $\mathcal{H}_{4,1-3}$, we adopt a mean-field like approach, replacing each possible contraction of operators with averages with respect to the quadratic, or ‘‘free’’ part, \mathcal{H}_2 [10, 11]. This procedure is equivalent to leading order perturbation theory in the interactions [12, 13]. For example, consider the scattering term

$$a_{k+q}^\dagger a_{k'-q}^\dagger a_{k'} a_k \approx \langle a_{k+q}^\dagger a_{k'} \rangle a_{k'-q}^\dagger a_k + \langle a_{k'-q}^\dagger a_k \rangle a_{k+q}^\dagger a_{k'} \\ + \langle a_{k+q}^\dagger a_k \rangle a_{k'-q}^\dagger a_{k'} + \langle a_{k'-q}^\dagger a_{k'} \rangle a_{k+q}^\dagger a_k \\ + \langle a_{k+q}^\dagger a_{k'-q}^\dagger \rangle a_{k'} a_k + \langle a_{k'} a_k \rangle a_{k+q}^\dagger a_{k'-q}^\dagger.$$

Using that the expectation values satisfy $\langle a_k^\dagger a_{k'} \rangle \propto \delta_{k,k'}$ and $\langle a_k a_{k'} \rangle \propto \delta_{k,-k'}$ one finds

$$a_{k+q}^\dagger a_{k'-q}^\dagger a_{k'} a_k \approx (\delta_{q,0} + \delta_{k+q,k'}) (\langle a_k^\dagger a_{k'} \rangle a_k^\dagger a_k + \langle a_k^\dagger a_k \rangle a_{k'}^\dagger a_{k'}) \\ + \delta_{k,-k'} (\langle a_{k+q}^\dagger a_{-k-q}^\dagger \rangle a_{-k} a_k + \langle a_{-k} a_k \rangle a_{k+q}^\dagger a_{-k-q}^\dagger).$$

Combing this decomposition with the interaction vertex, as specified in Eq. (S5b), gives the expression

$$\mathcal{H}_{4,2-2} \approx \sum_k \left(\frac{1}{N} \sum_q V_{k,q,0} \langle a_q^\dagger a_q \rangle \right) a_k^\dagger a_k \\ + \frac{1}{2} \sum_k \left\{ \left(\frac{1}{2N} \sum_q V_{q,-q,k-q} \langle a_q a_{-q} \rangle \right) a_k^\dagger a_{-k}^\dagger + \text{H.c.} \right\},$$

where $V_{k,k',k'-k} = V_{k,k',0}$ and $V_{k,k',0} = V_{k',k,0}$ has been used to simplify the normal term, and shifting the momentum has been used to simplify the anomalous terms. The quartic terms thus appear as corrections to the A_k and B_k quadratic terms.

Next, consider the same manipulations for the anomalous boson terms, starting with

$$a_k^\dagger a_{k'}^\dagger a_q^\dagger a_{k+k'+q} \approx \langle a_k^\dagger a_{k'} \rangle a_q^\dagger a_{k+k'+q} + a_k^\dagger a_{k'}^\dagger \langle a_q^\dagger a_{k+k'+q} \rangle \\ + \langle a_k^\dagger a_q^\dagger \rangle a_{k'}^\dagger a_{k+k'+q} + a_k^\dagger a_q^\dagger \langle a_{k'}^\dagger a_{k+k'+q} \rangle \\ + \langle a_k^\dagger a_{k+k'+q} \rangle a_{k'}^\dagger a_q^\dagger + a_k^\dagger a_{k+k'+q} \langle a_{k'}^\dagger a_q^\dagger \rangle.$$

Using the fact that the expectations in this last equation are diagonal in \mathbf{k} (or skew-diagonal) [as in Eq. (S8)], we find

$$a_k^\dagger a_{k'}^\dagger a_q^\dagger a_{k+k'+q} \approx \delta_{k,-k'} (\langle a_k^\dagger a_{-k} \rangle a_q^\dagger a_q + a_k^\dagger a_{-k}^\dagger \langle a_q^\dagger a_q \rangle) \\ + \delta_{k,-q} (\langle a_k^\dagger a_{-k} \rangle a_{k'}^\dagger a_{k'} + a_k^\dagger a_{-k}^\dagger \langle a_{k'}^\dagger a_{k'} \rangle) \\ + \delta_{k',-q} (\langle a_k^\dagger a_k \rangle a_{k'}^\dagger a_{-k'}^\dagger + a_k^\dagger a_k \langle a_{k'}^\dagger a_{-k'}^\dagger \rangle).$$

Combining this decomposition with the anomalous interaction vertex, $D_{k,k',q}$ from Eq. (S5c), and using the permutation symmetry of its arguments, we find

$$\mathcal{H}_{4,3-1} \approx \sum_k \left(\frac{1}{2N} \sum_q D_{q,-q,k} \langle a_q^\dagger a_{-q}^\dagger \rangle \right) a_k^\dagger a_k \\ + \frac{1}{2} \sum_k \left(\frac{1}{N} \sum_q D_{k,-k,q} \langle a_q^\dagger a_q \rangle \right) a_k^\dagger a_{-k}^\dagger.$$

These terms thus also appear as corrections to the A_k and B_k in the quadratic part of the Hamiltonian. Note that the Hermitian conjugate term of this $\mathcal{H}_{4,3-1}$ also contributes, with its contribution read off from the expression above.

$$\begin{aligned} \mathcal{H}_{4,1-3} \approx & \sum_k \left(\frac{1}{2N} \sum_q D_{q,-q,k}^* \langle a_q a_{-q} \rangle \right) a_k^\dagger a_k \\ & + \frac{1}{2} \sum_k \left(\frac{1}{N} \sum_q D_{k,-k,q}^* \langle a_q^\dagger a_q \rangle \right) a_{-k} a_k. \end{aligned}$$

Finally, we can summarize all of these contributions as corrections δA_k and δB_k to the original A_k and B_k of quadratic \mathcal{H}_2 origin and write

$$\delta A_k = \frac{1}{N} \sum_q \left[V_{k,q,0} \langle a_q^\dagger a_q \rangle + \frac{1}{2} \left(D_{q,-q,k} \langle a_q^\dagger a_{-q} \rangle + \text{c.c.} \right) \right], \quad (\text{S10a})$$

$$\delta B_k = \frac{1}{N} \sum_q \left[D_{k,-k,q} \langle a_q^\dagger a_q \rangle + \frac{1}{2} V_{q,-q,k-q} \langle a_q a_{-q} \rangle \right]. \quad (\text{S10b})$$

In terms of these corrections, the renormalized spectrum is given by

$$\Omega_k \equiv \sqrt{(A_k + \delta A_k)^2 - (B_k + \delta B_k)^2}. \quad (\text{S11})$$

These corrections can be evaluated using the bare, free averages from Eq. (S8), though this approach leads to divergences (see Sec. III F). Alternatively, they can be evaluated self-consistently, with the averages in Eq. (S8) computed using $(A_k + \delta A_k)$, $(B_k + \delta B_k)$ and Ω_k instead of A_k , B_k and ω_k , which cures the divergences.

C. Pseudo-Goldstone gap

The effects of the interactions on the pseudo-Goldstone mode can now be examined. The energy of the $\mathbf{k} = \mathbf{0}$ mode is given by

$$\Delta \equiv \Omega_0 = \sqrt{2KS (\delta A_0 + \delta B_0) + \delta A_0^2 - \delta B_0^2}. \quad (\text{S12})$$

For small corrections $\delta A_0, \delta B_0$, Δ above can be approximated by (the leading term)

$$\Delta \approx \sqrt{2KS} \sqrt{\delta A_0 + \delta B_0}. \quad (\text{S13})$$

In the quantum limit where $T \ll \omega_k$, the corrections $\delta A_k, \delta B_k$ are $O(S^0)$ and thus the gap scales as $\Delta \propto \sqrt{S}$. In the classical limit where $T \gg \omega_k$ the corrections scale as $\delta A_k, \delta B_k \sim O(T/S)$ and thus the gap scales as $\Delta \propto \sqrt{T}$, independent of S .

D. Pseudo-Goldstone Linewidth

To estimate the scaling of the pseudo-Goldstone mode linewidth with temperature, we consider the magnon self-

energy [11] at $\mathbf{k} = \mathbf{0}$ near $\omega = 0$, which takes the form

$$\Sigma(\mathbf{0}, 0) \equiv \begin{pmatrix} \delta A_0 & \delta B_0 \\ \delta B_0^* & \delta A_0^* \end{pmatrix},$$

where δA_0 and δB_0 are corrections due to magnon-magnon interactions. Perturbatively, we expect that

$$\delta A_0 = a_1 T + a_2 T^2 + \dots, \quad (\text{S14a})$$

$$\delta B_0 = b_1 T + b_2 T^2 + \dots, \quad (\text{S14b})$$

where the $O(T)$ corrections (computed in this work) encoded in a_1, b_1 are both real. The quasi-normal modes, corresponding to the locations of poles of the magnon Green's function [11, 14], are determined from eigenvalues of $\sigma_z \mathbf{M}_0^{\text{eff}}$ where

$$\mathbf{M}_0^{\text{eff}} = \begin{pmatrix} A_0 + \delta A_0 & -A_0 + \delta B_0 \\ -A_0 + \delta B_0^* & A_0 + \delta A_0^* \end{pmatrix}.$$

Up to and including terms of $O(T^2)$, the quasi-normal mode frequency is thus given by

$$\begin{aligned} \text{Re } \Omega_0 & \approx \sqrt{2A_0(a_1 + b_1)} \sqrt{T} \\ & + \left(\frac{a_1^2 - b_1^2 + 2A_0(\text{Re } a_2 + \text{Re } b_2)}{4A_0(a_1 + b_1)} \right) T^{3/2} + \dots, \\ \text{Im } \Omega_0 & \approx (\text{Im } a_2) T^2 + \dots. \end{aligned}$$

We thus see that the linewidth, determined by $\text{Im } \Omega_0$, is expected to scale as T^2 .

E. Self-Consistent Mean-Field Theory (SCMFT)

To include the effects of the magnon-magnon interactions self-consistently, we define the ‘‘mean-fields’’

$$n_k \equiv \langle a_k^\dagger a_k \rangle, \quad d_k \equiv \langle a_k^\dagger a_{-k}^\dagger \rangle. \quad (\text{S15})$$

Using Eq. (S10), new values of n_k and d_k can then be computed by iteratively updating A_k and B_k to

$$\begin{aligned} A'_k & = A_k + \frac{1}{N} \sum_q \left[V_{k,q,0} n_q + \frac{1}{2} \left(D_{q,-q,k} d_q + D_{q,-q,k}^* d_q^* \right) \right], \\ B'_k & = B_k + \frac{1}{N} \sum_q \left[D_{k,-k,q} n_q + \frac{1}{2} V_{q,-q,k-q} d_q^* \right], \end{aligned}$$

which, using Eq. (S8), results in updated values of n_k and d_k . This process is repeated until the variables n_k and d_k have converged to the desired precision across the full Brillouin zone.

For the calculations reported here, and in the main text, convergence was considered reached when the sum of all absolute values of the changes in n_k and d_k in Eq. (S15) over the Brillouin zone between iterations was less than 10^{-10} . To launch the iterative process, the mean-fields, n_k and d_k for each \mathbf{k} , are initially set to a value of $1/2$, though the precise choice of initial value was not found to affect the final results. Following this approach, we calculate the PG gap for several system

sizes, using a discrete sum of the Brillouin zone with $N = L^2$ points. We then extrapolate the gap in the system size to obtain the result in the thermodynamic limit ($N \rightarrow \infty$). The finite size scaling of the PG gap using SCMFT is shown in Fig. S2.

F. Cancellation of divergences in the pseudo-Goldstone gap

Since the non-interacting LSWT spectrum is gapless, we must be mindful of infrared divergent contributions to δA_0 and δB_0 . Let us first address this issue in the simplest context, bare perturbation theory in the quartic interactions.

We focus on the classical limit where $\omega_k \ll T$, but similar considerations apply in the full quantum case at finite temperature; since $\omega_k \rightarrow 0$ as $k \rightarrow \mathbf{0}$, there is always a regime in k near the zone center where the frequency is small relative to temperature, even in the quantum limit. Consider the corrections, Eq. (S10), in the thermodynamic limit ($N \rightarrow \infty$), replacing the discrete sums with integrals. At $k = \mathbf{0}$, this gives [using Eq. (S8)]

$$\delta A_0 = \int \frac{d^2q}{(2\pi)^2} \frac{T}{\omega_q^2} [V_{0,q,0}A_q - D_{q,-q,0}B_q], \quad (\text{S16a})$$

$$\delta B_0 = \int \frac{d^2q}{(2\pi)^2} \frac{T}{\omega_q^2} \left[D_{0,0,q}A_q - \frac{1}{2}V_{q,-q,-q}B_q \right], \quad (\text{S16b})$$

where the integral is over the Brillouin zone $-\pi \leq q_x, q_y \leq \pi$ (the lattice spacing has been set to one). At small q , the spectrum is approximately linear in q with

$$\omega_q = S \sqrt{2K(J|q|^2 + Kq_y^2)} + O(|q|^2)$$

and thus the factor $T/\omega_q^2 \propto 1/|q|^2$ is singular as $|q| \rightarrow 0$. The numerators of the integrals in Eq. (S16) remain finite in this limit, with

$$V_{0,q,0}A_q - D_{q,-q,0}B_q = -\frac{SK^2}{2} + O(|q|^2),$$

$$D_{0,0,q}A_q - \frac{1}{2}V_{q,-q,-q}B_q = +\frac{SK^2}{2} + O(|q|^2).$$

One therefore finds that both δA_0 and δB_0 are logarithmically divergent. Explicitly, integrating over a region $2\pi/L < |q| < \Lambda \ll \pi$

$$\int_{2\pi/L < |q| < \Lambda} \frac{d^2q}{(2\pi)^2} \frac{1}{\omega_q^2} = \frac{1}{4\pi S^2 K \sqrt{J(J+K)}} \ln\left(\frac{L\Lambda}{2\pi}\right). \quad (\text{S17})$$

Since the upper cutoff is chosen to satisfy $\Lambda \ll \pi$, the divergent contributions to δA_0 and δB_0 take the form

$$\delta A_0 = -\frac{TK \ln L}{8\pi S \sqrt{J(J+K)}} + (\text{reg.}), \quad (\text{S18a})$$

$$\delta B_0 = +\frac{TK \ln L}{8\pi S \sqrt{J(J+K)}} + (\text{reg.}), \quad (\text{S18b})$$

where (reg.) stands for terms that remain finite as $L \rightarrow \infty$. Interestingly, while δA_0 and δB_0 are each $\ln L$ divergent, the *sum*

$(\delta A_0 + \delta B_0)$ which appears in the expression for the pseudo-Goldstone gap [Eq. (S13)], Δ , is finite. This can be made more explicit by carrying out the same expansions for $(\delta A_0 + \delta B_0)$,

$$\delta A_0 + \delta B_0 = \int \frac{d^2q}{(2\pi)^2} \frac{T}{\omega_q^2} \left[2K^2 S(q_x^2 - q_y^2) + O(|q|^4) \right]. \quad (\text{S19})$$

The $O(|q|^2)$ term in the ω_q^2 denominator is thus compensated by a corresponding $O(|q|^2)$ in the numerator of Eq. (S19). However, note that this cancellation *only occurs at leading order* in $\delta A_0, \delta B_0$. The complete expression $\sqrt{(A_0 + \delta A_0)^2 - (B_0 + \delta B_0)^2}$, which incorporates higher-order contributions, remains logarithmically divergent. Similarly, the leading corrections from bare perturbation theory to Ω_k at *non-zero* k are also divergent.

Since the bare perturbation theory diverges, except for the leading temperature dependence of the PG gap at $q = \mathbf{0}$, in order to obtain the full temperature dependence of the interaction corrections to Ω_q , we proceed with a self-consistent approach. This way, the equation for the corrections δA_0 and δB_0 become

$$\delta A_0 = \int \frac{d^2q}{(2\pi)^2} \frac{T}{\Omega_q^2} \left[V_{0,q,0}(A_q + \delta A_q) - D_{q,-q,0}(B_q + \delta B_q) \right],$$

$$\delta B_0 = \int \frac{d^2q}{(2\pi)^2} \frac{T}{\Omega_q^2} \left[D_{0,0,q}(A_q + \delta A_q) - \frac{1}{2}V_{q,-q,-q}(B_q + \delta B_q) \right],$$

where the renormalized spectrum Ω_q arises from evaluating the averages in Eq. (S8) self-consistently. In such a self-consistent mean-field theory, the spectrum Ω_q ‘‘already’’ contains a finite gap at $q = \mathbf{0}$. The gap acts as an effective infrared cutoff rendering the integrals in Eq. (S17) finite. The disappearance of the divergence then manifests itself in the cancellation of the leading (self-consistent) dependence on the gap Δ .

To see this explicitly, consider the self-consistent spectrum which, for small q , takes the form

$$\Omega_q = \sqrt{2KS^2(J|q|^2 + Kq_y^2)} + \Delta^2 + O(|q|^2).$$

For sufficiently small Δ , the integration region can be divided into two parts: $|q| \gtrsim k_0$ and $|q| \lesssim k_0$ such that

$$\Omega_q \approx \begin{cases} \Delta, & |q| \lesssim k_0, \\ S \sqrt{2K(J|q|^2 + Kq_y^2)}, & |q| \gtrsim k_0. \end{cases}$$

Roughly, the boundary separating these regions scales as

$$k_0 \sim \frac{\Delta}{SK} \propto \sqrt{T} \quad (\text{S21})$$

when $K \gtrsim J$. Alternatively, k_0 is the wave-vector at which the bare spectrum ω_k becomes comparable to the interaction induced gap, Δ . The primary change to the spectrum, and thus to δA_0 and δB_0 , occurs for $|q| < k_0$. Carrying out the integration in Eq. (S17) over the region responsible for its divergent contributions, we find they are rendered finite. Explicitly,

$$\int_{k_0 < |q| < \Lambda} \frac{d^2q}{(2\pi)^2} \frac{1}{\Omega_q^2} \sim \frac{\ln(KS\Lambda/\Delta)}{4\pi S^2 K \sqrt{J(J+K)}}.$$

Given that $\Delta \propto \sqrt{T}$, this contribution to the integral now scales as $-\ln T$. Thus the divergence has been cured in the individual corrections δA_0 and δB_0 . We note that the $\ln(\Lambda/\Delta) \sim -\ln T$ terms cancel in the sum $(\delta A_0 + \delta B_0)$ which controls the leading contribution to the gap [similarly to Eq. (S13)] and the result from bare perturbation theory is recovered. In this way, bare perturbation theory for the asymptotic \sqrt{T} scaling of the pseudo-Goldstone gap is well-defined and divergence free, and matches the results from the SCMFT calculations. Note that the region $0 < |q| < k_0$ gives only a finite contribution that goes as

$$\int_{0 < |q| < k_0} \frac{d^2 q}{(2\pi)^2} \frac{1}{\Omega_q^2} \sim \frac{k_0^2}{4\pi\Delta^2} \sim \text{const.},$$

since $k_0 \propto \Delta$.

G. Logarithmic corrections to magnetization

While the contributions $\propto \ln T$ cancel in the leading parts of Δ , they reappear explicitly in static quantities such as the magnetization. In the classical limit, the net magnetization [Eq. (S9)] is given by

$$M = S - T \int \frac{d^2 k}{(2\pi)^2} \frac{A_k}{\omega_k^2}, \quad (\text{S22})$$

in the thermodynamic limit ($N \rightarrow \infty$). Like the bare corrections δA_0 and δB_0 in Eq. (S16), in LSWT M has a (logarithmic) infrared divergence, given that ω_k scales linearly with k at small $|k|$, while A_k tends to the constant $A_0 = KS$. Naïvely, this would indicate the destruction of the order, as happens when there is a true symmetry-protected Goldstone mode [15].

To resolve this divergence, we must include the dynamically generated pseudo-Goldstone gap. The expression for M in the SCMFT can be obtained from Eq. (S22), via the replacements $\omega_k \rightarrow \Omega_k$ and $A_k \rightarrow A_k + \delta A_k$. Explicitly,

$$M = S - T \int \frac{d^2 k}{(2\pi)^2} \frac{A_k + \delta A_k}{\Omega_k^2}, \quad (\text{S23})$$

where, again, Ω_k is the self-consistent spectrum with pseudo-Goldstone gap Δ . Following the same strategy as in Sec. III F,

we approximate the self-consistent spectrum, Ω_k , over the three pertinent regions of reciprocal space

$$\Omega_k \approx \begin{cases} \Delta, & 0 < |k| \lesssim k_0 \\ S \sqrt{2K(J|k|^2 + Kk_y^2)}, & k_0 \lesssim |k| \lesssim \Lambda \\ \omega_k, & |k| \gtrsim \Lambda \end{cases} \quad (\text{S24})$$

The integral defining M is then split into three parts

$$\int \frac{d^2 k}{(2\pi)^2} = \int_{0 < |k| < k_0} \frac{d^2 k}{(2\pi)^2} + \int_{k_0 < |k| < \Lambda} \frac{d^2 k}{(2\pi)^2} + \int_{|k| > \Lambda} \frac{d^2 k}{(2\pi)^2}.$$

The first and second integrals depend on temperature through $\Delta \propto \sqrt{T}$ and $k_0 \sim \Delta/(KS)$ [see Eq. (S21)]. The last integral is over wave-vectors large enough such that the interaction corrections are minor and, therefore, this contribution to the integral has no additional temperature dependence. The correction to M from this last (third) term is thus $\propto T$.

For the region $|k| \lesssim \Lambda$, we approximate $A_k + \delta A_k \approx KS$, leaving the two contributions

$$\begin{aligned} \int_{0 < |k| < k_0} \frac{d^2 k}{(2\pi)^2} \frac{KST}{\Delta^2} &= \frac{T}{4\pi KS}, \\ \int_{k_0 < |k| < \Lambda} \frac{d^2 k}{(2\pi)^2} \frac{KST}{2KS^2(J|k|^2 + Kk_y^2)} &= \frac{T \ln(KS\Lambda/\Delta)}{4\pi S \sqrt{J(J+K)}}. \end{aligned}$$

The renormalized spectrum has thus yielded two additional contributions to M : one that adds an additional part $\propto T$ and another new, and perhaps most interesting, part, $\propto T \ln T$, and where we used $\Delta \propto \sqrt{T}$.

To summarize, the magnetization at low temperatures takes the form

$$M = S - c_1 T - c_2 T \ln T + \dots, \quad (\text{S25})$$

where c_1 and c_2 are temperature independent constants. The logarithmic $T \ln T$ dependence arises from the temperature dependence of the pseudo-Goldstone gap, Δ . As $T \rightarrow 0$, both of these temperature dependent terms go to zero (as it should classically) and the system becomes fully polarized with $M \rightarrow S$. Hence true long-range order is induced by ObTD, with the lurking infrared divergences tamed by the ObTD-induced PG gap, Δ .

[1] J. D. Alzate-Cardona, D. Sabogal-Suárez, R. F. L. Evans, and E. Restrepo-Parra, “Optimal phase space sampling for Monte Carlo simulations of Heisenberg spin systems,” *Journal of Physics: Condensed Matter* **31**, 095802 (2019).
[2] Michael Creutz, “Overrelaxation and Monte Carlo simulation,” *Phys. Rev. D* **36**, 515–519 (1987).
[3] M. E. J. Newman and G. T. Barkema, *Monte Carlo methods in statistical physics* (Clarendon Press, Oxford, 1999).
[4] J. R. Dormand and P. J. Prince, “A family of embedded Runge-Kutta formulae,” *Journal of Computational and Applied Mathematics* **6**, 19–26 (1980).

[5] K. Ahnert and M. Mulansky, “Odeint – solving ordinary differential equations in C++,” *AIP Conference Proceedings* **1389**, 1586–1589 (2011).
[6] K. Ahnert and M. Mulansky, “Boost C++ Library: Odeint,” (2012).
[7] J. C. Bowman and M. Roberts, “FFTW++: A fast Fourier transform C++ header class for the FFTW3 library,” (2010).
[8] A. Auerbach, *Interacting Electrons and Quantum Magnetism*, Graduate Texts in Contemporary Physics (Springer New York, 1998).
[9] Jeffrey G. Rau, Paul A. McClarty, and Roderich Moess-

- ner, “Pseudo-Goldstone gaps and order-by-quantum disorder in frustrated magnets,” *Phys. Rev. Lett.* **121**, 237201 (2018).
- [10] H. Bruus and K. Flensberg, *Many-Body Quantum Theory in Condensed Matter Physics: An Introduction*, Oxford Graduate Texts (Oxford University Press, Oxford, 2004).
- [11] J.P. Blaizot and G. Ripka, *Quantum Theory of Finite Systems* (MIT Press, Cambridge, 1986).
- [12] P. D. Loly, “The Heisenberg ferromagnet in the selfconsistently renormalized spin wave approximation,” *Journal of Physics C: Solid State Physics* **4**, 1365–1377 (1971).
- [13] A. V. Chubukov, S. Sachdev, and T. Senthil, “Large- S expansion for quantum antiferromagnets on a triangular lattice,” *Journal of Physics: Condensed Matter* **6**, 8891–8902 (1994).
- [14] M. E. Zhitomirsky and A. L. Chernyshev, “Colloquium: Spontaneous magnon decays,” *Rev. Mod. Phys.* **85**, 219–242 (2013).
- [15] P. M. Chaikin and T. C. Lubensky, *Principles of Condensed Matter Physics* (Cambridge University Press, 1995).